Possible Bose-condensate behavior in a quantum phase originating in a collective excitation in the chemically and optically doped Mott-Hubbard system UO_{2+x}

Steven D. Conradson,[1,*] Tomasz Durakiewicz,[1] Francisco J. Espinosa-Faller,[2] Yong Q. An,[1,†] David A. Andersson,[1] Alan R. Bishop,[1] Kevin S. Boland,[1] Joseph A. Bradley,[1,3] Darrin D. Byler,[1] David L. Clark,[1] Dylan R. Conradson,[1] Leilani L. Conradson,[1] Alison L. Costello,[1] Nancy J. Hess,[4] Gerard H. Lander,[5] Anna Llobet,[1] Mary B. Martucci,[1] Jose Mustre de Leon,[6] Dennis Nordlund,[7] Juan S. Lezama-Pacheco,[1,‡] Thomas E. Proffen,[1,§] George Rodriguez,[1] Daniel E. Schwarz,[1] Gerald T. Seidler,[3] Antoinette J. Taylor,[1] Stuart A. Trugman,[1] Trevor A. Tyson,[8] and James A. Valdez[1]

[1]*Los Alamos National Laboratory, Los Alamos, New Mexico 87545, USA*
[2]*Universidad Marista de Merida, Merida, Yucatan 97300, Mexico*
[3]*University of Washington, Seattle, Washington 98195, USA*
[4]*Pacific Northwest National Laboratory, Richland, Washington 99352, USA*
[5]*Institute for Transuranium Elements, Karlsruhe, 76344, Germany*
[6]*Cinvestav-Merida, Merida, Yucatan, 97310, Mexico*
[7]*SLAC National Accelerator Laboratory, Menlo Park, California 94025, USA*
[8]*New Jersey Institute of Technology, Newark, New Jersey 07102, USA*

(Received 2 February 2012; revised manuscript received 15 April 2013; published 23 September 2013)

X-ray pair distribution function (pdf) and U L_3 extended x-ray absorption fine structure (EXAFS) and neutron pdf measurements that give identical results for UO_2 show U(VI)-oxo moieties with x rays for mixed valence U_4O_9 and U_3O_7, in contrast to the neutron data that indicate only U(V) sites with no short U-O bonds as well as other differences. In addition, although the EXAFS spectra of UO_2 are essentially identical at 30, 100, and 200 K, those of the UO_{2+x} compounds exhibit different nearest-neighbor U-O distributions at each temperature. Further tunneling polaron-type behavior is found in the broadening of the features of the O K-edge x-ray absorption spectra (XAS) of the UO_{2+x} compounds. Raman spectra of powders also show a large increase in scattering cross section with increasing O content that would originate in a change in the electronic structure that increases the overall polarizability. The XAS and Raman also show that U_4O_9 does not behave as a linear combination of the UO_2 and U_3O_7 fluorite endpoints. The properties induced by mobile rather than static charged quasiparticles were explored by optical pumping of the metal-to-metal charge-transfer transition. The temperature dependence of 4.71 eV pump–1.57 eV probe reflectivity on UO_2 that initially populates the U 6*d*-dominated portion of the upper Hubbard band (UHB) shows a sharp 28-μsec lifetime peak at 25 K that may be associated with the fluctuations of its antiferromagnetic transition. Pumping at 3.14 eV into the 5*f*-dominated portion of the UHB shows an analogous 2.8-μsec peak but also a plateau bracketing this peak that ends in a cusp at 50–60 K and an abrupt change in the hardening rate of a novel 12–15 GHz phonon that is the signature for the quasiparticle quantum phase. The different results for the different excitation channels indicate a highly specific nonthermal relaxation mechanism. These results constitute the first observation of a distinct phase of photoinduced quasiparticles that is sufficiently coupled to the lattice to undergo a gap-opening transition. When the intragap state is probed with a terahertz time domain spectroscopy (TTDS) measurement 33 psec after a 3.14 excitation pulse, it shows increased absorption in the 0.5–1.1 THz range with a decrease in temperature from ~30 to 10 K instead of the expected decrease, a result consistent with the presence of a condensate. These results are too extreme to originate in the dynamical, nonadiabatic, coupled charge-transfer–phonon/tunneling polaron scenario previously used for doped Mott-Hubbard insulators with intermediate electron-phonon coupling and therefore indicate novel physics. One possibility that could cause all of these behaviors is that a collective, dynamical, charge transfer-coupled Peierls distortion involving the 2 U(V) $\leftrightarrow$ U(IV) + U(VI)-oxo excitation occurs coherently over an entire domain to cause the atoms in this domain to condense into a system with Bose-Einstein or Bose-Einstein-Hubbard properties.

DOI: 10.1103/PhysRevB.88.115135 PACS number(s): 74.20.Mn, 61.43.−j, 71.36.+c, 87.15.hp

Because of its role as both nuclear fuel and subsequent environmental contaminant,[1] UO_2 is one of the most thoroughly studied materials. It is also, however, scientifically fascinating as a strongly correlated, large Hubbard gap,[2–5] Mott insulator that is easily rendered partially filled in the fluorite structure with a continuous O:U ratio from 2.0 through 2.33–2.5 (see Refs 6 and 7). Although this class of materials is poorly understood, it is expected to exhibit interesting polaron physics. For mixed valence UO_{2+x}, this physics intersects with unusual structural chemistry. The molecular complexes of U in aqueous systems are highly constrained, exhibiting spherical geometries in the (III) and (IV) valences but transforming to the highly oblate trans-dioxo configuration with its opposing very short (1.7–1.8 Å) triply bonded pair of O ions for U(VI).[8] Condensed oxide and oxyhydroxide phases, however, exhibit a much greater variety of local environments and behaviors. The extended spatial extent of the 5*f* electrons in combination with the f^2 configuration of UO_2 result in dynamic Jahn-Teller distortions[9–13] among a large number of low lying electronic states.[2,14–17] These couple strongly with the phonons of the fluorite structure,[18–20] the magnons from the unpaired spins,[11] and the higher order multipoles to produce phonons of mixed

vibrational-quadrapolar-acoustic character that cause avoided crossings and other complications in the phonon-dispersion curves.[21] These explain the complex antiferromagnetic (AFM) transition, in which the dynamical, uncorrelated, 1-**k** Jahn-Teller distortions of the O atoms become increasingly coherent upon cooling to form the static 3-**k** order of the AFM state[11] at 30.8 K[22,23] with its 0.014 Å displacements of the O ions.[24]

Much larger structural variations occur in U(VI)-containing oxides. If the ternary uranates[6,25–29] are included, condensed oxides and oxyhydroxides display an essentially continuous range of U(VI)-O bond lengths from 1.7 through 2.5 Å. The extreme example is UO_3 and its allotropes. In its ambient temperature α form that can be considered as layered U_3O_8 with some of the bridging oxos transformed to terminal because removing one-ninth of the U ions breaks the continuity of the [001] O-U-O-U-O chains,[30] these terminal U-oxo bonds are an extremely short 1.69 Å. At 375 °C, however, UO_3 transforms to the δ phase composed of fully symmetric UO_6 octahedra with U-O = 2.08 Å.[31] This quasiconservation of the volume by changes in the Poisson ratio of the oblate sphere as the U-oxo and equatorial bonds move in opposite directions is characteristic of these U compounds, with the 30% bond length variation in the uranyl species being an extremely large value for any system.

The wide range of U(VI)-O distances implies that the single minimum in the overall potential that limits the structures of the molecular complexes is much less constrained in the extended solids, being essentially flat between the radial and highly distorted regimes depending on the nuances of the local environment. One result of this decoupling of the typical relationship between valence and bonding is that the binary uranium-oxygen system, with the O:U ratio continuous from 1.5–3.0, is arguably the most complicated one we know,[32,33] with the number of crystallographically distinct phases reported as 16 between $UO_{1.5}$ to UO_3 (see Ref. 34) but also as many as 22 just from UO_2 up.[35] This ambiguity in counting and defining a phase corroborates the complexity of the behavior.

Of particular interest is the microscopic mechanism for the addition of O to UO_{2+x} that has been evolving for almost 50 years.[36–38] One problem in resolving it is the disorder in the two higher single-phase compounds that occur in the flourite region of the phase diagram, cubic U_4O_9, and tetragonal U_3O_7, whose lattice constants differ by less than 1% from that of UO_2. Although the long-range average structure of the U sublattice is conserved to give good diffraction patterns, disorder in the O positions has prevented exact crystal-structure mapping of even their high temperature phases.[39–43] In addition, U_3O_7 possesses a poorly defined phase boundary composition[7] and variable tetragonal distortion that can change over time,[44] while x-ray diffraction (XRD) of U_4O_9 shows contractions of the lattice relative to UO_2 that are often less than the differences between multiple reports for the same stoichiometries.[38,39,45–48]

With the addition of O to form UO_{2+x}, the adventitious O aggregates at low x ($\sim$0.04) to form U_4O_9-like domains for $x < 0.25$ and then U_3O_7-like ones for $x > 0.25$ so that intragrain-phase separation occurs in the regions of the phase diagram with U:O ratios between the single phase UO_2, U_4O_9, and U_3O_7 compounds.[6] At elevated temperatures, however, enhanced displacements and entropy-driven cube vertex-interstitial substitutions of the O result in merging of these domains into disordered single phases. Models of the oxidation mechanism typically involve addition of adventitious O into the cubic holes of the open fluorite-lattice concomitant with displacements of original O ions into neighboring holes, leaving the cube vertices vacant.[37,38,40,46,49–52] The most well-known model invokes the formation of cuboctahedral structures.[37–39,51] More recent reports indicate greater stability for di-interstitial defects that dimerize into quad-interstitial ones. These are similar to the cuboctahedrons,[52,53] but with a 2:1 instead of a 1:1 ratio of adventitious to native displaced/interstitial O ratio. Both models,[51,52] as well as neutron pair distribution function (pdf) results,[41] give a broad, single-peaked U-O nearest-neighbor (NN) distribution centered around the 2.36 Å distance of UO_2 with no U-O distances below 2.10–2.15 Å. The conservation of the U sublattice is consistent with the formation of small, immobile polarons.[54,55]

A problem and controversy arose when x-ray absorption fine structure (XAFS) spectroscopy showed that UO_{2+x}, $0 \leqslant x \leqslant 0.25$ contained U(VI)-oxo, or uranyl, groups and substantial anharmonic U-U disorder.[56–58] This is analogous to the Pu(V)-oxo groups found by XAFS in PuO_{2+x}.[59,60] Subsequent neutron scattering[41,42] and ion channeling[42] measurements and calculations[7,52,53] confirmed the original U(V)-O $\geqslant$ 2.15 Å assignment. In fact, the highly oblate geometry of the UO_2^{2+} moiety implied by XAFS is incompatible with the UO_2 structure, lacking a placement in the lattice that would not cause substantial strain. We have, however, performed calculations that show that, as in UO_3, O ions in environments with U vacancies are displaced toward the remaining U ions until, in the extreme case, they form a terminal oxo group when only a single U ion is within bonding range. This process in UO_{2+x} would require large displacements of many of the U ions, but another difference between the XAFS and neutron-scattering results was that XAFS found precisely this type of disorder in the U-U distribution.[56,57]

We now resolve this controversy over the properties and effects of charge defects or inhomogeneities in UO_{2+x} via additional structural and other measurements on UO_{2+x}, supplemented by optical pump-probe experiments on $UO_{2.00}$. In the first of these, measurements of local and electronic structure were performed on O-doped UO_{2+x} samples in which the adventitious O forms lattice defects that would inhibit transport as well as rendering the material mixed valence. In the second, fsec-resolved optical reflectivity and psec-resolved terahertz time-domain spectroscopy (TTDS) transmission measurements were performed after transient charge inhomogeneities were induced in a $UO_{2.00}$ crystal by optical pumping of the metal-to-metal charge transfer transitions. Since the material remains perfectly stoichiometric, the photoinduced polaronic quasiparticles are not pinned by lattice defects and may therefore exhibit enhanced mobility and contribute to transient transport and correlated properties, as was observed in cuprates.[61] Although we have recently reported an initial investigation of this experiment, we found some deviations from the expected behavior that merited these further studies.[62]

The results of these experiments reported here all identify unexpected, unusual, and even unique behaviors of polaronic

quasiparticles in UO_2 that demonstrate that, although their interaction with the lattice is intermediate between metallic and fully localized small polarons, their interactions with each other are quite strong. Although the neutron and x-ray structural measurements on UO_2 give identical results, demonstrating that the stoichiometric material behaves classically, the two probes find different local structures in U_4O_9 and U_3O_7, and XAFS measurements at several temperatures show fluctuations in the U-O distribution over a very wide temperature range. Such discrepancies in functionally layered, mixed-valence, correlated transition metal compounds were interpreted as indicative of a dynamic tunneling polaron as the origin of the observed lattice instability.[63–69] Corroborating this interpretation for UO_{2+x} are our O K-XAS results that show that the electronic states in UO_{2+x} differ from those of other U oxides by being substantially broadened and losing the separation between the U $5f$ and $6d$ states,[70] another result predicted for a dynamical system.[67] These results supplement the observation of the predicted[4,71] significant dispersion of the $5f$ states below the Fermi level in UO_2 (see Ref. 5) that would promote its ability to interact with other electrons and atoms. These findings in UO_{2+x} are novel because, first, it would extend this phenomenon to a new class of materials and, second, the associated lattice distortion is far too large for the polaron tunneling description applied to cuprates *et al.*,[65,67,72–74] necessitating a new mechanism. The results for the quasiparticle lifetimes and the accompanying phonon spectra show unprecedented behaviors that are best interpreted as aggregation and self-organization of the photoinduced quasiparticles into a coherent structure. This excitonic or polaronic condensate subsequently undergoes at least one gap-opening phase transition at 50–60 K and possibly a second one near the sharp peak in the lifetimes at 20–25 K that is associated with the AFM transition. An exciting possibility that explains these results is a polaronic Bose system in a periodic potential with a repulsive onsite interaction and tunneling.[75,76] Its persistence to high temperatures might be possible because the condensation originates not from all of the particles being in the ground state but rather from coherence induced by the 2 U(V) $\leftrightarrow$ U(IV) + U(VI) disproportionation excitation occurring collectively within domains of polaronic quasiparticles undergoing the dynamical, charge transfer-coupled, Peierls distortion between the U(V) and U(VI)-oxo states.

I. EXPERIMENTAL AND ANALYTICAL PROCEDURES

A. Preparation of materials

Ultrapure UO_2 was prepared by crystallizing $UO_2(O_2)$ from aqueous solution, which was converted to UO_3 by heating in air at 400 °C, followed by reduction with H_2 at 500 °C. The amorphous UO_3 was obtained in this way. It is assumed that this is locally identical to α UO_3 (see Ref. 30) that results from heating at a somewhat higher temperature,[77] differing only in the U vacancies being disordered. U_4O_9 for the nonresonant inelastic x-ray scattering (NIXS) measurement was made by heating a mixture of the appropriate amounts of U_3O_8 and UO_2 in a sealed quartz tube at 1000 °C for 15 days. The O XAS samples of $UO_{2.25}$/U_4O_9, $UO_{2.09}$, and $UO_{2.16}$ were made from the controlled oxidation of a commercial high-purity UO_2 starting material and verified by XRD. U_3O_7 was made by oxidizing UO_2 in air at 225 °C for 24 hours. Orthorhombic U_3O_8 was prepared by heating $UO_2(O_2)$ in air at 800 °C and verified by XRD. $Cs_2UO_2Cl_4$ was prepared by known methods, as described in Ref. 78. Purity was checked by XRD, and, for the fluorite compounds, purity was checked by the neutron and x-ray scattering (see Supplemental Material[79]) and U L_3 XAFS. All compounds were handled anaerobically. Samples for the NIXS, O XAS, and U L_3 XAFS were ground and cast into polystyrene films under inert atmosphere, as reported previously.[80,81] The samples for NIXS were around 70 wt-% of the material, 30 wt-% polystyrene. O K-XAS samples were much more dilute, around 5 wt-%, and were mixed with C powder before casting as a suspension in the polystyrene-toluene solutions into ca. 2×6 mm wells in individual Cu blocks, with ~20 Å of C sputtered onto their surfaces for protection and conduction. Samples for neutron scattering were placed in the standard vanadium cans. Samples for x-ray scattering were placed in thin-walled glass capillaries. Single crystal samples for optical measurements were obtained from a UO_2 boule, available at Los Alamos National Laboratory. The sample for TTDS was prepared by polishing a piece from this boule to obtain a plate with parallel sides ~400-μ thick.

B. Neutron and x-ray scattering

Time-of-flight neutron-scattering measurements were performed at the Neutron Powder Diffractometer end station at the Lujan Neutron Scattering Center, Los Alamos National Laboratory. Approximately 5 g of each compound was loaded into a vanadium holder. The UO_2 and U_3O_7 were run at ambient temperature, the U_4O_9 at 20 K. For all three compounds, x-ray scattering measurements were performed at the Stanford Synchrotron Radiation Lightsource (SSRL) at end station 10-2 at 27 000 eV (0.4593 Å) at ambient temperature, using a few mg of material packed into thin-walled, 200–400 μ-diameter quartz capillary tubes. The same Ge detector was used for all measurements, with the analyzer window set to include both the elastic and the Compton peaks. The scattering data were analyzed by conventional procedures with the PDFgetX,[82] PDFgetN,[83] PDFgui,[84] and GSAS[85] programs. Neutron-diffraction patterns were refined using the Rietveld method, as was the x-ray pattern of UO_2. The diffraction patterns of U_4O_9 and U_3O_7 were indexed, but full refinements were not attempted because of the disorder in the structures that has historically prevented full solution of the structures. The diffraction patterns of U_4O_9 were fit using the results from Ref. 40. The diffraction patterns of U_3O_7 were fit by allowing the UO_2 structure to undergo a tetragonal distortion. The starting points for the analyses of the pdfs were these structures. The pdfs were also fit as a sum of Gaussian functions, which do not impose any constraints on the relative positions, amplitudes, and widths of the peaks and would therefore be less susceptible to artifacts caused by more extensive disorder. The neutron- and x-ray scattering data were analyzed identically to minimize the possibility of differences between them caused by artifacts. Standard procedures were used, including the normalizations,

Compton-scattering corrections, conversion from $F(Q)$ to $S(Q)$, etc., using the algorithms contained in these analysis programs. Fourier transforms for both neutrons and x rays were performed over identical ranges in Q, with $Q_{max} = 21$ Å^{-1} because the intensity of the x-ray signal was deemed insufficient beyond. The Fourier ripple that is caused by this termination of the transform range is relatively larger in the x-ray pdfs because of the smaller x-ray cross section for the U-O pair. This ripple is also calculated by the analysis programs based on Q_{max} and is therefore included in the fits. Detailed results from the analyses are contained in the Supplemental Material.[79]

C. U L_3 x-ray absorption fine structure

U L_3 XAFS spectroscopy measurements were also performed on end station 10-2 at SSRL. Samples containing approximately 10 mg of U were ground, suspended in a solution of polystyrene in toluene, and placed in the 2.5 × 20 mm slots in an aluminum holder where the toluene was allowed to evaporate. The holder was attached to the cold finger of an open-cycle liquid He refrigerator. The temperatures are those recorded for the end of the cold finger; in practice, the sample temperature is higher, especially at lower temperatures, so that the nominal 30 K will be above the Neel temperature and the sample in the paramagnetic phase. The energies were calibrated by measuring the spectrum of a Y metal foil within the same scan with the first inflection point of this standard defined as 17 032.08 eV. The extended x-ray absorption fine structure (EXAFS) data were analyzed with standard methods using the software developed at Los Alamos. U-O and U-U phase shifts and amplitudes for curve fitting were calculated using the FEFF 7 (see Ref. 86) code, which appears to give better results than those from FEFF 8 (see Ref. 87) for actinides. Errors in the metrical parameters were determined by calculating the increase in the least squares error resulting from removing a particular shell and then varying each parameter until the error in the total fit had increased by 10% of that amount. However, in disordered materials such as UO_{2+x}, we believe that rather than the curve-fitting results indicating the presence of the specific shells it is much better to use the overall result as a gross description of the U partial pdf that, including thermal broadening, is likely to exhibit continuous neighbor atom density over a broad distance range.

D. Non-resonant Inelastic X-ray Scattering

The O K-NIXS on UO_2 and U_3O_7 were measured at the same time as the $O_{4,5}$ NIXS spectra previously reported,[81] were from the same materials, and used the same preparation and experimental methods.[80] All NIXS measurements were taken using the lower energy resolution inelastic x-ray scattering (LERIX) user facility at the PNC/XOR 20-ID undulator beamline of the Advanced Photon Source[88] using a double-crystal Si (111) monochromator with incident photon flux of $\sim 10^{12}$/s. The net energy resolution (full width at half-maximum[FWHM]) of the monochromator and the LERIX analyzer crystals is 1.3 eV, as determined from the width of the elastic-scattering line. NIXS data extraction and processing followed methods reported previously.[88,89] The dipole approximation to the NIXS cross section was verified by the independence of the O K-edge shape over the range of q reported, so that the spectra shown here are the summed counts from six different detectors spanning from $q \sim 3.3$ to 4.8 arb. units. The typical measurement time per data point is 80 s, which yields ∼5000 counts in the q-integrated edge step above the ∼60 000 counts from background due to the valence Compton scattering. Although the polystyrene matrix darkened in color during the measurement, the NIXS data were unaffected, as determined by comparing spectra as the total dose accumulated.

E. O K x-ray absorption spectra

The O K fluorescence yield (FY) XAS measurements were also performed as reported previously,[80] except that the UO_{2+x}/U_4O_9 spectra were measured on beam line 10-1 instead of 8-2. Room temperature O K-edge XAS data were recorded at SSRL at beamline 8-2, utilizing bending magnet radiation and a spherical grating monochromator, under ring conditions of 3.0 GeV and 85–100 mA. A standard vacuum system was used, except that for U a 1200 Å carbon window was used to isolate the chamber from the upstream instrumentation and ring. The incident radiation was monitored using a Au grid with 80% transmission. The fluorescence was measured using two International Radiation Detector XUV100-type photodiodes coated with 1000 Å of aluminum in normal incidence. This was accomplished by placing the photodiodes facing the sample with a 3-mm gap between them for the passage of the beam. The diodes were 5–10 mm from the sample and were mounted in a cavity in a grounded copper block to prevent electrical interference. The total electron yield as the photocurrent and FY data for the spectra of the various compounds showed no sign of radiation damage. The UO_{2+x} and U_4O_9 were measured on beam line 10-1 with the sample turned 45° and the diode at a right angle relative to the beam. FY data were converted to absorbance by dividing the diode by the grid current. They were normalized by fitting a line through a flat region below the initial rise in absorbance and offsetting the spectra so that the value of this line at 533 eV equaled zero and, multiplied by a factor so that the value of a second line fit over the flat region above the absorption edge features from approximately 550–590 eV, was unity at this same energy. In some spectra, sloping backgrounds beyond the spectral peaks caused the absorption to be below one in this region, resulting in a diminution in the amplitudes of these peaks as well. However, since we only compare relative amplitudes within a spectrum, this has no effect on the interpretation of the results.

F. Raman spectroscopy

Raman spectra were collected on a few milligrams of polycrystalline uranium oxide loaded into glass double-well slides and sealed with acrylic coverslips in an Ar-filled atmosphere-controller chamber with less than 1 ppm O_2. The polycrystalline samples were placed on the stage of a confocal Raman microscope and imaged in white light using a video camera. A split cell allowed imaging of the focused laser beam onto the individual polycrystalline grains using the video image. Using a 100 × objective, the focused laser beam has

an approximately 1.5 micron spot size. The Raman spectra were excited using approximately 10 mW of 532-nm laser excitation, and the scattered light was collected in backscattering geometry. To maximize the discrimination of the Raman signal from the sample sitting on the glass slide, the confocal aperture was adjusted to reduce the collected Raman intensity by 10%. The scattered light was passed through a high-resolution triple spectrometer in subtractive mode and illuminated a liquid nitrogen-cooled charge coupled device detector with 2000 × 800 pixels. The entrance and exit slits were set at 150 microns. For each sample, the Raman spectrum was acquired from 100 to 1800 cm^{-1} using multiple 600 cm^{-1} spectral frames that were combined together to span the entire spectral region. The Raman signal was acquired for 4 minutes for each frame or approximately 12 minutes for the entire spectral region. Due to the low-laser power used, the Raman spectra were acquired for a minimum of 3 hours and averaged together. Prior to averaging, spectra collected early in the run were compared to those at the end of the run to detect signs of sample degradation under the laser excitation. All spectra were collected at room temperature.

G. Ultrafast time-resolved optical pump probe

The experiment was performed identically to the previous one on a single crystal of UO_2 from the same boule.[62] The pump energies were, respectively, the frequency-doubled 3.14-eV fundamental of the 250-kHz Ti:sapphire regenerative laser corresponding to excitation into the $5f$-dominated portion of the upper Hubbard band at pump fluences of 50, 100, and 200 $\mu J/cm^2$, the frequency-tripled beam at 4.71 eV, corresponding to excitation into the $6d$-dominated portion of the upper Hubbard band at 16 $\mu J/cm^2$; and the probe energy fundamental at 1.57 eV within the gap.

H. Optical pump-terahertz probe

For this experiment, a single crystal of UO_2 was polished parallel to the (001) plane to a thickness of 400 microns, at which point the polishing was stopped because of the fragility of the material. This thickness was confirmed by the measurement. In the TTDS system, a mode-locked Ti:sapphire laser beam of pulse duration of 30 fs, repetition 1 kHz, fluence of 266 $\mu J/cm^2$, and center wavelength of 800 nm was split into two beams. The weaker beam transmitted through a thin ZnTe crystal for the generation of a terahertz pulse of the wavelength in the range of 0.2–2.5 THz was used as the probe. The terahertz beam was focused on the UO_2 crystal sample with a focused beam spot size of 3.5 mm. The stronger beam that was used to excite the $2U5f^2 \rightarrow U5f^1 + U5f^3$ metal-to-metal charge transfer transition in UO_2 was collimated into a smaller beam for the second-harmonic generation (SHG) by a $BaBO_3$ crystal. The SHG beam size was about 5 mm on the UO_2 crystal, and it was overlapped onto the terahertz beam on the sample. The actual beam used was the echo after reflecting off the crystal faces because this passed through the photoexcited volume three times to boost its contribution to the transmitted beam. The terahertz beam transmitted through the UO_2 crystal was collimated and then focused onto another ZnTe crystal for the detection of the terahertz pulse by electro-optic sampling. The birefringence of ZnTe was modulated by the electric field of the terahertz pulse and then detected by a polarization analysis system, including a quarter-wave plate, a polarization prism, and two balanced detectors. The probe terahertz beam was modulated by a mechanical chopper operating at 500 Hz, and the signals from the balanced detectors are fed in a lock-in amplifier for phase-sensitive detection. The UO_2 sample was mounted on a cold finger in a cryostat cooled by liquid helium to access varying temperatures from 4 to 500 K. A translation stage was used to vary the time delay between the pump and the probe pulses arriving at the UO_2 sample. Positive delay times were assigned to data where the pump pulse arrives at the UO_2 sample before the probe. A delay time of 33 psec was selected.

I. Density functional theory calculations of U(VI)-oxo stability

Density functional theory (DFT) calculations for oxidation of bulk and surface UO_2 were performed with the Vienna *Ab initio* Simulation Package (VASP)[90–92] applying the projector-augmented wave (PAW) method.[93,94] The Lichtenstein formulation of the LDA + U (local-density approximation) methodology was applied to the U $5f$ electrons.[95] The U and J values were set to U = 4.5 eV and J = 0.51 eV, respectively.[96] We used a 2 × 2 × 2 supercell (96 atoms) expansion of the cubic fluorite unit cell to study bulk oxygen clusters. The volume was held constant at the calculated volume of UO_2. All static calculations applied a 2 × 2 × 2 Monkhorst-Pack k-point mesh, and the plane-wave cutoff was set to 400 eV. We also verified that increasing the plane-wave cutoff to 500 eV and, allowing for volume relaxation, does not alter any of our conclusions. The internal structural parameters were relaxed until the Hellmann-Feynman forces on each ion were sufficiently small (<0.02 eV/Å). The details of our static calculations are further discussed in Ref. 52. In order to minimize complications arising from the prevalence of metastable electronic solutions for the LDA + U method,[13,97,98] all simulations apply reduced structural symmetry, and the symmetry switch in VASP was explicitly turned off in all simulations. For each case, multiple simulations were performed in order to find the solution with lowest energy. Further, *ab initio* molecular dynamics (MD) simulations were performed in order to efficiently sample a range of structural configurations for each type of initial structure. The MD simulations applied reduced k-point mesh and a lower plane-wave cutoff in order to increase the computational efficiency. The UO_2 (111) surfaces were studied using a periodic slab of UO_2 ($[0.5\ 0.0\ -0.5]_{Fluorite}$, $[-0.75\ 0.75\ 0.0]_{Fluorite}$, $[1.0\ 1.0\ 1.0]_{Fluorite}$) separated by vacuum along the third dimension. For this setup, a 2 × 2 × 2 Monkhorst-Pack k-point mesh was applied. Using this methodology, we determined the UO_2 surface oxidation energy to be −2.28 eV/O after correcting for the overbinding of O_2 molecules within DFT (see Ref. 52 for details) to be compared to −1.59 eV/O for single interstitials and −2.33 eV/O for the most stable quad-clusters. The extra oxygen at the UO_2 (111) surface exhibits a NN bond length of 1.85 Å, which is similar to that found in experiments. The fact that surface oxidation is more favorable than bulk oxidation based on single interstitials means that initial oxidation will

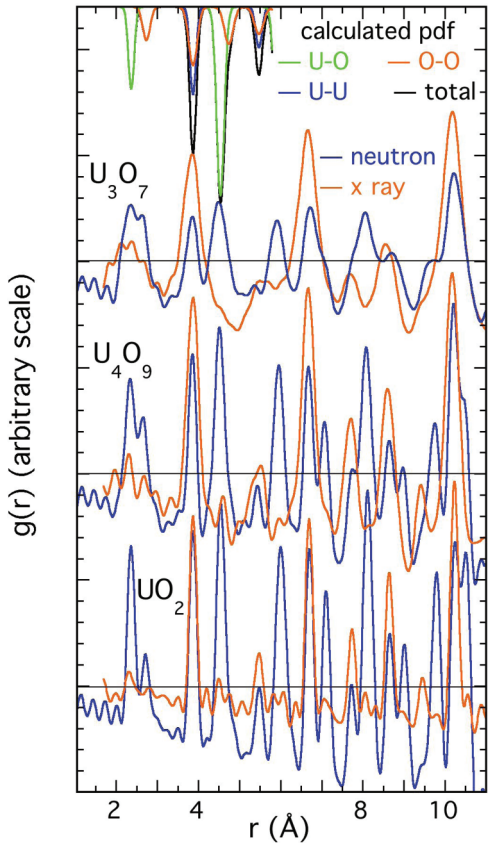

FIG. 1. (Color online) Neutron and x-ray pdfs of UO_2 (bottom), U_4O_9 (center), U_3O_7 (top), and a portion of the calculated neutron pdf of UO_2 (inverted across upper margin). The data are scaled arbitrarily to maximize their amplitudes within this figure.

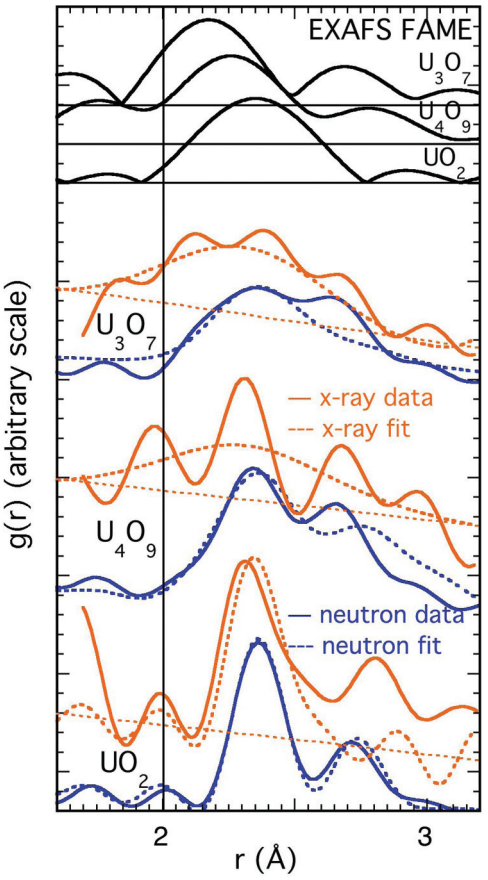

FIG. 2. (Color online) Neutron and x-ray pdfs of UO_2 (bottom), U_4O_9 (center), and U_3O_7 (upper), with a fit of the NN U-O and O-O pairs (dashed) to the structure of the UO_2 data and two-Gaussian fits (described in text) to the U_4O_9 and U_3O_7 data and the FAME moduli of the EXAFS at 30 K (top). The slanted baselines typical of x-ray pdfs are shown as are the horizontal baselines of the FAME results. The vertical line at 2 Å facilitates discerning the areas of the triangles that represent the atomic density of uranyl-type U-oxo pairs that are defined by the data, these baselines, and this line at 2 Å.

occur at such imperfections. The surface-oxidation mechanism and formation of quad-clusters are essentially degenerate. This balance opens the possibility that bulk UO_2 exhibiting large enough distortions of the U sublattice, such as the (partial) U_3O_8 transition discussed in this manuscript, could host terminal oxos.

II. RESULTS

A. Determination of local structure by x-ray and neutron pdf and EXAFS spectroscopy

Reconciling the disagreement between the U(VI)-oxo moieties in the UO_{2+x} structure found by XAFS[56–58] and the much smaller distortions in the more spherical U(V) environment from the neutron pdfs[41] begins with comparing the pdfs of UO_2, U_4O_9, and U_3O_7, where material from the same batch has been measured with both neutrons and x rays (Fig. 1). As described in the Methods section, the data were analyzed to ensure that effects of the range and other parameters would be identical. Allowing for the greater magnitude of the neutron form factor for O and the larger Fourier ripple because of the relatively low signal from the x rays, the pdfs of UO_2 from the two probes are identical and match the crystal structure. The number of peaks, their positions, widths, and relative amplitudes in the x-ray and neutron data are within experimental error and show no signs of disorder. UO_2 is therefore well behaved in the classic crystallographic sense, with the experimental pdf matching the one calculated from the crystal structure, demonstrating no aperiodic local lattice distortions.

The pdfs of mixed valence U_4O_9 and U_3O_7 show that the addition of O broadens and reduces the amplitudes of the peaks. Beyond this common trend, however, and in definite contrast to UO_2, the x-ray and neutron pdfs of U_4O_9 and U_3O_7 show significant differences. The widths of the U-U peak at 3.85 Å are 0.17 and 0.16 Å for, respectively, the neutron and x-ray pdfs of UO_2. They increase to 0.18 (neutron) and 0.31 Å (x ray) for U_4O_9, continuing to 0.27 (neutron) and 0.46 Å (x ray) in U_3O_7. The greater width of the peaks in the x-ray pdf continues for the other U-U pairs at the longer distances. In addition, there are indications of peaks in the x-ray pdf at, e.g., 5.5 Å, etc., which are not observed in the neutron results.

The specific question of oxo-type moieties in UO_{2+x} is addressed in a closer inspection of the NN U-O (and O-O) region (Fig. 2). The effects of Fourier ripple and background residuals on the relatively low amplitude U-O peaks in

the x-ray pdfs were countered by fitting the pdf data with the UO_2 structure. Complex, anharmonic, possibly multisite distributions are therefore approximated and fit by single Gaussians, so that in the 1.5–3.2 Å regions there is only one Gaussian for the O-O pair and a second one that fits the entire U-O distribution. This process has the effect of averaging the ripple to extract a more visually accessible, albeit single-peaked, description of the U-O distribution. The neutron pdf of UO[2] recapitulates the crystal structure. The x-ray pdf is adequate for the U-O pair. It shows a shift of the O-O position so that the peak at 2.8 Å is apparently ripple, which is not unexpected because of the very low amplitude of O-O pairs with x rays. The NN U-U and more distant pairs continue to be adequately fit with both neutrons and x rays so that the direct measurements via the pdfs of UO_2 therefore display nothing unusual.

The addition of O causes the same trend in the NN O distribution from the neutron pdfs as in the full range, the U-O + O-O peaks become broader and lower from UO_2 through U_4O_9 to U_3O_7. These comparisons of the data, augmented by the curve-fits, clearly show that even with this doping-induced disorder and broadening there is no O density in the neutron pdfs below 2.0 Å, and any below 2.1 Å is the edge of a broad peak centered at a higher value, corroborating the previous report.[41] In contrast, the x-ray pdfs from UO_{2+x} display much wider peaks. The left sides of these peaks extend well below 2.0 Å based on the area of the triangle composed of the data or fit, the vertical line at 2.0 Å, and the baseline of the fit. Inspection of the fits and comparison of the pdfs with that of UO_2 thus definitively show substantial U-O atomic density starting at the 1.7–1.8 Å uranyl distance. This effect is mirrored on the far side of the 2.36 Å U-O peak of UO_2; U-O pairs extend through 2.6 Å or higher. Another observation is that the centers of these peaks trends toward lower r across the series.

Corroboration by the EXAFS is obtained directly from Fourier analysis by maximum entropy (FAME) that removes the U-O phase shift so that the resulting transform gives peaks at the real U-O distances rather than the phase shifted ones. Although the overall pattern is still subject to interference and, for this NN, background residuals, multiple U-O shells with small separations are clearly visible (Fig. 2). FAME analysis thus duplicates the behavior of the x-ray pdfs. Substantial U-O density below 2.0 Å in terms of the area of the same triangle bounded by the modulus, the horizontal baseline, and the vertical line at 2.0 Å does not occur for UO_2 but is exhibited by the UO_{2+x} compounds accompanied by a downward shift in the population/r^2-weighted main peak. In addition, the EXAFS and pdfs of U_4O_9 and U_3O_7 show the same shift of the principal peak and fit to lower r relative to UO_2. This shift is greater for U_3O_7 than for U_4O_9, which is consistent with the identification by the curve-fits of a U-O shell at around 2.14 Å. Although its position is somewhat variable, its separation from the original UO_2-type shell at 2.3 Å is just at or below the resolution of the fitting range. Therefore, rather than being a discrete shell, the combination of these two shells model a wide, continuous distribution of U-O bonds that peak at a distance significantly lower than in UO_2. These results verify both the x-ray pdfs and our earlier report on the EXAFS of UO_{2+x} (see Ref. 57).

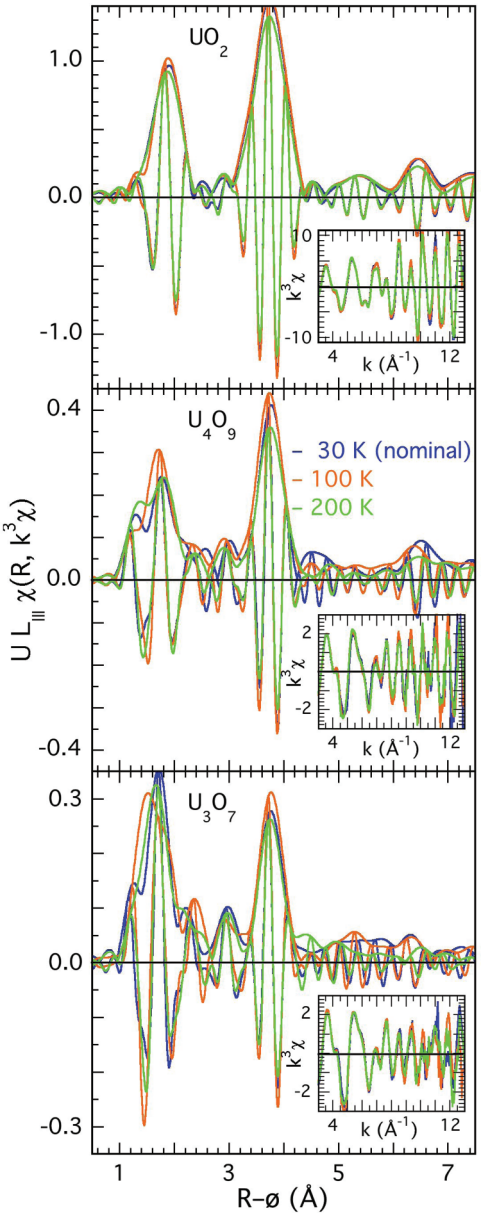

FIG. 3. (Color online) EXAFS spectra ($\chi(R)$ representation, k = 3.2–13.0 Å^{-1}, insets are $k^3\chi(k)$) of indicated compounds at indicated temperatures. Note change of vertical scale.

B. Temperature dependence of local structure by EXAFS

EXAFS measurements at nominal values of 30, 100, and 200 K (Fig. 3) were performed to search for additional dynamical anomalies in the structures of these compounds. The UO_2 spectra show the rigidity that is expected in the absence of any crystallographic phase transitions over this temperature range, displaying almost perfect overlap within the experimental uncertainty of its $\chi(R)$ spectra (Fig. 3) except for the expected small decreases in the amplitudes at higher temperatures. As in the pdfs, UO_2 thus exhibits conventional behavior.

The NN U contributions at R = 3.8 Å in the spectra of U_4O_9 and U_3O_7 are also relatively temperature independent and always fit well with a single U shell, although their highly reduced amplitudes relative to UO_2 verify the anharmonic U-U disorder in the mixed-valence compounds.[57] The NN O

TABLE I. Curve-fitting results for variable temperature EXAFS. The fitting range is for $k = 2.4$–15.0 Å^{-1}, k^3 weighting. The asterisk denotes fixed parameter at this value.

	O Shells							U Shell
UO_2			8.6 atoms					15.2 atoms
30 K			2.35 Å					3.83 Å
			$\sigma = 0.089$					$\sigma = 0.059$
UO_2			8.5 atoms					9.4 atoms
100 K			2.35 Å					3.83 Å
			$\sigma = 0.087$					$\sigma = 0.031$
UO_2			8.8 atoms					12.2 atoms
200 K			2.35 Å					3.84 Å
			$\sigma = 0.093$					$\sigma = 0.055$
U_4O_9	0.5 atoms	0.8 atoms	4.1 atoms	0.4 atoms		0.7 atoms	1.4 atoms	7.6 atoms
30 K	1.68 Å	2.02 Å	2.26 Å	2.47 Å		3.24 Å	3.42 Å	3.88 Å
	$\sigma = 0.107$	$\sigma = 0.083$	$\sigma = 0.101$	$\sigma = 0.003$		$\sigma = 0.000$	$\sigma = 0.050^*$	$\sigma = 0.088$
U_4O_9	0.1 atoms		4.4 atoms		0.5 atoms	0.4 atoms	0.7 atoms	9.3 atoms
100 K	1.65 Å		2.26 Å		2.87 Å	3.14 Å	3.36 Å	3.87 Å
	$\sigma = 0.074$		$\sigma = 0.123^*$		$\sigma = 0.050^*$	$\sigma = 0.001$	$\sigma = 0.050^*$	$\sigma = 0.095$
U_4O_9	0.4 atoms		4.7 atoms		0.3 atoms	0.8 atoms	0.8 atoms	6.2 atoms
200 K	1.69 Å		2.28 Å		2.91 Å	3.14 Å	3.39 Å	3.86 Å
	$\sigma = 0.079$		$\sigma = 0.132^*$		$\sigma = 0.050^*$	$\sigma = 0.060^*$	$\sigma = 0.060^*$	$\sigma = 0.091$
U_3O_7	0.2 atoms	0.9 atoms	2.4 atoms	1.2 atoms			0.9 atoms	5.7 atoms
30 K	1.66 Å	2.14 Å	2.26 Å	2.43 Å			3.44 Å	3.87 Å
	$\sigma = 0.050$	$\sigma = 0.074$	$\sigma = 0.062$	$\sigma = 0.049$			$\sigma = 0.052$	$\sigma = 0.094$
U_3O_7	0.2 atoms	1.4 atoms	3.4 atoms	0.5 atoms	0.4 atoms		0.5 atoms	9.1 atoms
100 K	1.67 Å	2.12 Å	2.28 Å	2.48 Å	2.85 Å		3.39 Å	3.88 Å
	$\sigma = 0.079$	$\sigma = 0.059$	$\sigma = 0.079$	$\sigma = 0.040$	$\sigma = 0.000$		$\sigma = 0.053$	$\sigma = 0.109$
U_3O_7	0.1 atoms	1.1 atoms	3.6 atoms		0.3 atoms	0.5 atoms	1.2 atoms	5.0 atoms
200 K	1.74 Å	2.17 Å	2.31 Å		2.90 Å	3.21 Å	3.43 Å	3.86 Å
	$\sigma = 0.060^*$	$\sigma = 0.060^*$	$\sigma = 0.118$		$\sigma = 0.060^*$	$\sigma = 0.060^*$	$\sigma = 0.060^*$	$\sigma = 0.085$

contributions for U_4O_9 and U_3O_7, however, display complicated patterns at $R = 1.0$–2.7 that undergo substantial variations, indicating temperature-driven shifts of a subset of the NN O atoms. Curve-fits of these spectra (Table I) reproduce the finding that the relatively large feature at $R = 1.2$ Å is the contribution from an O at ∼1.65–1.7 Å, while the small feature at this position in the spectrum of $UO_{2.00}$ is a side lobe of the principal peak.[57] Although the number of these oxo- or uranyl-type atoms is small, with the caveat that this value is highly correlated with and dependent on the corresponding Debye-Waller factor (Table I), their contribution to the spectra is accentuated by the dependence of the amplitude on the inverse square of the absorber-scatterer distance.

For both U_4O_9 and U_3O_7, the shoulder at $R = 1.2$ Å is diminished at 100 K because the modulus of the $R = 1.8$ Å peak shifts lower while the feature at $R = 2.4$ Å is highest at this temperature, suggesting that the O displacements in these nonfluorite shells are similar in the two compounds. The curve-fitting results corroborate this interpretation for the $R = 2.4$ Å feature, with the fits of both the U_4O_9 and U_3O_7 spectra requiring an O neighbor shell around 2.9 Å at 100 and 200 but not at 30 K. Extracting the U-O distribution via curve-fitting analysis is more difficult because of the extensive disorder that will include overlap of the distances at and below the resolution limit of the spectra and destructive interference of the EXAFS waves so that the metrical parameters from the fits should not necessarily be taken literally. This is evident in the FAME results. The curve-fits and FAME both show a larger U(VI)-oxo contribution for U_4O_9 than U_3O_7, which implies that the change in structure with the addition of O is not a continuous process. The U_4O_9 phase is therefore not a fortuitous point between UO_3 and the terminal fluorite $U_3O_{7(.33)}$ but must instead be where the specific mechanism for the addition of O is altered. The defect structure of U_4O_9 supports a relatively large number of U(VI)-oxo groups, but after the structure is saturated with this particular conformation to produce the homogeneous material with this composition, the addition of further groups to form U_3O_7 gives a different configuration that partially suppresses them. As expected, these changes are echoed in the longer range structure beyond 4 Å that is unchanged for UO_2. The discrete rearrangements of the NN O atoms shown by these spectra therefore clearly demonstrate that at least some of the O in mixed valence UO_{2+x} occur as multisite U-O distributions with low barriers between the minima (100 K = 9 meV) that promote significant shifts in their positions with changes in temperature.

C. Oxygen K-edge NIXS, FY, and XAS measurements

A second type of static experiment on UO_{2+x} is the O K-edge XAS that gives information on the electronic structure

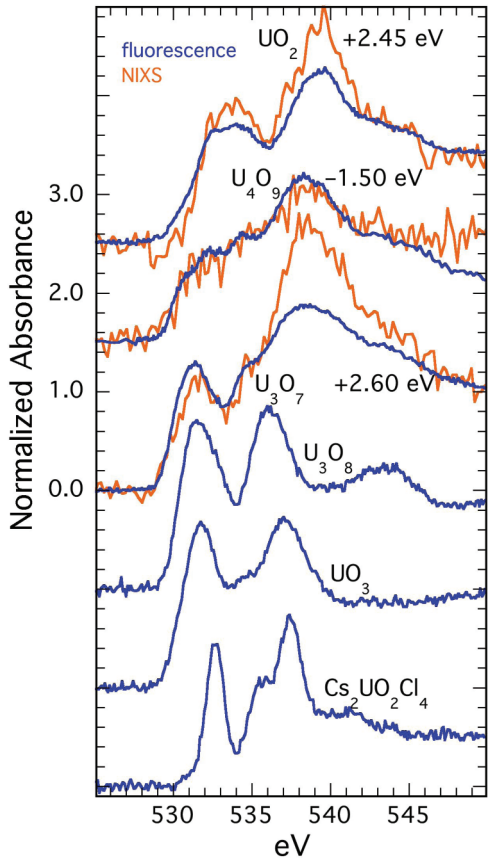

FIG. 4. (Color online) Fluorescence-yield O K x-ray absorption and nonresonant inelastic scattering spectra of indicated compounds. The numbers for the oxides indicate the shift to align the FY spectra with the NIXS. The spectra of the other compounds are uncalibrated. The NIXS spectra are not modified by self-absorption and give more accurate amplitudes for the spectral features.

of the unfilled states above the Fermi level. Insofar as these low-energy measurements are susceptible to artifacts from contamination or modifications of the surfaces[3,99–103] and reduction of the peak amplitudes by self-absorption, the spectra of the UO_{2+x} materials were validated by NIXS. The spectra of U_3O_8, amorphous UO_3 that is expected to have the same local structure and spectrum as layered α-UO_3 (see Ref. 102), and $Cs_2UO_2Cl_4$ (see Ref. 78) are included for comparison (Fig. 4). These are corroborated by the O XAS that have already been reported for these compounds and whose spectral fall within the range of the peaks that we have observed for different preparations of UO_2 (see Ref. 70).

The spectra of the last three are notable in exhibiting two large peaks with additional fine structure that are well separated by a pronounced dip between them that descends to or below the baseline absorbance at higher energy. The spectrum of UO_2 (see Refs. 70, 99, and 102) has a distinctly similar appearance, especially when measured on single crystals[3] where the amplitude of the lower energy feature rises to that of the higher energy one, although its features are broader and spread out over a wider range relative to these other oxides. We have attributed this to several sources that should all diminish as the charge on the U increases.[70] The assignments of the spectral features are almost identical because of the mirroring of the symmetry between the cubic-spherical geometry of UO_2 and the quasioctahedral U environments in the molecular U(VI)-oxo or uranyl complexes that are similar to the U site geometries in higher valence layered U oxides. The consensus is that the lower peak consists of transitions to final states that are principally U 5*d* in character that occur in the lower energy portion of the upper-Hubbard band and that the higher energy peak consists of transitions to states of primarily U 6*d* character.[3,4,71,99,102,104] The ionization energy is within the 6*d* manifold[78] and therefore the transition to the continuum occurs within this second feature. One issue with the assignments is the shoulder on the lower peak that is the lowest energy feature in all of these spectra that was left unassigned in $Cs_2UO_2Cl_4$ (see Ref. 78) but has been attributed to the U 5*f* states in UO_2 (see Refs. 3, 99, and 104), in which case the remainder of the assignments do not correspond well to the spectra.[70] What is relevant here is that this feature occurs even in filled shell compounds and therefore cannot be an O^- radical,[105] consistent with the electropositive character of U(IV) and (V).

The DFT + U calculations show that the neutron-scattering based structures of U_4O_9 and U_3O_7 that present relatively small distortions of the cubic geometry maintain this same pattern of separated 5*f* and 6*d* states in their O XAS spectra.[70] The experimental spectra, however, obviously do not display this behavior. Using the more accurate amplitudes from the NIXS, the low energy peak of the U_3O_7 spectrum is greatly diminished even as the higher energy one increases in both amplitude and width. This minimal display of two peaks does not even occur in the U_4O_9 spectrum where there is a continuous set of ascending features. In addition, the width of the spectra as the energy between the first inflection point from the lower energy peak and the higher energy peak that reflects the total dispersion of the U 5*f* and 6*d* states composing the upper Hubbard band[70] is 5.4 eV for $Cs_2UO_2Cl_4$, 6.5 eV for UO_3, 5.8 eV for U_3O_8, and 7.8 eV for UO_2 but 8.5 eV for U_4O_9 and 8.6 eV for U_3O_7, which would be yet wider relative to the others if there was an adequate way to define the upper limit of the high energy peak.

Based on the examples of U_3O_8 and UO_3, inhomogeneous line broadening because of local distortions to the perfect geometries does not appear to have much effect on the width of the spectra. Since spin-orbit coupling has been shown to give only part of these peak widths, the other factors that would give the observed spectral broadening are multiplet splitting and the Coulomb interaction. Insofar as both of these are reduced as the charge on the U increases, these parameters can explain the trend observed from UO_2 to U_3O_8 and the two U(VI)-oxo compounds. The spectral features of U_4O_9 and U_3O_7, however, display the opposite pattern, increasing in width even as O is added. We also find that when the features are deconvoluted by fitting the spectra with Gaussians, the total density of states (DOS) of UO_2 calculated by hybrid DFT, DFT + U, and FEFF give similar results that correspond well with the experimental measurements.[70] However, as with the structural measurements, DFT + U calculations for UO_{2+x} based on structures with minimized energies that give pdfs very close to those measured with neutrons do not give results that correspond with these experimental spectra. In summary, both the behavior of these spectra and the results from calculations indicate that the changes in the U_4O_9 and U_3O_7 spectra relative

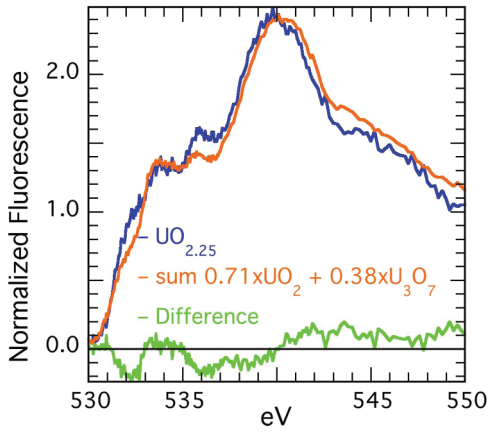

FIG. 5. (Color online) Fluorescence yield spectrum of U_4O_9 compared with indicated weighted sum of the endpoint UO_2 and U_3O_7 spectra. The bottom trace is the difference between the data and this sum.

to UO_2 must therefore originate in properties outside of the conventional ones that are successful in explaining the DOS of UO_2.

Another result from the calculations is that in both the cuboctahedral and the di-interstitial models of the adventitious O addition, the defects are identical throughout the fluorite region so that the compounds are differentiated simply by how the larger numbers of defects are organized over longer distances.[39,52,53,106] U_4O_9 should therefore give a spectrum intermediate between UO_2 and U_3O_7. The U_4O_9 spectrum can be emulated by a combination of the UO_2 and U_3O_7 spectra that are the endpoints for the fluorite structure, but different combinations only match one region and not its entirety. The example shown (Fig. 5) demonstrates that the lower energy portion that does not display a peak and in which the valley between the two peaks is replaced by a flat region with some small features can be obtained by a combination of these two spectra. This is accomplished, however, with a combination of the endpoints that is far from the actual U_4O_9 stoichiometry. In addition, the excessive UO_2 contribution causes the energy of the principal peak in the fit to occur at a higher value than in the data. The U_4O_9 spectrum may therefore contain some of the same components that constitute the endpoint spectra; however, if so, then the underlying electronic states must interact so as to transfer spectral weight between them.

This anomalous behavior for the hypervalent fluorites poses the question of its origin. The NIXS proves that it is not surface contamination, nor can it be self-absorbance because that suppresses amplitudes proportionately to their amplitude relative to the bulk absorbance beyond the edge used for normalization. The O K-XAS of a crystal of PuO_2 that also sustains hypervalent species showed amplitude variations that were postulated to originate in variations in the local O content but that were also much smaller than observed here.[103] This leaves as the most likely explanation that the electronic structure behaves analogously to the crystal structure, exhibiting the mixing of both the ground and excited electronic states that causes the overall DOS to broaden as predicted for the intrinsic dynamics associated with tunneling polarons.[67]

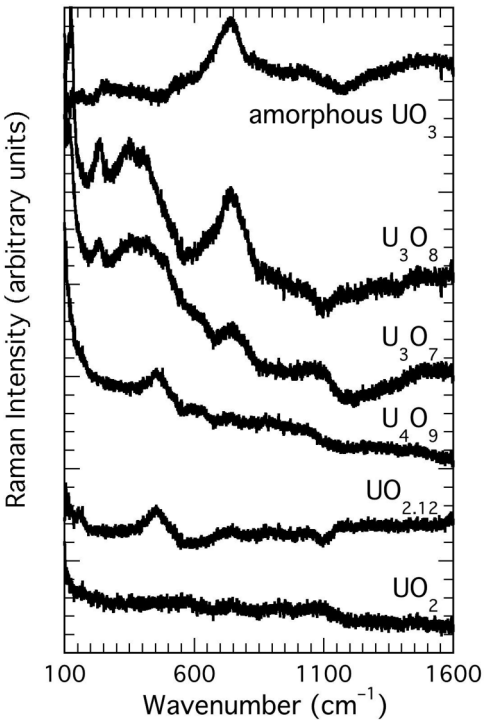

FIG. 6. Raman spectra of indicated U oxides.

D. Raman spectroscopy

Another pertinent measurement of UO_{2+x} is the Raman spectra. Those of UO_2 crystals and polished polycrystalline UO_{2+x} pellets are easily measured,[20,48,107,108] as are the higher nonfluorite oxides.[109] In contrast, the powders we used that were the same samples subjected to the structural measurements gave somewhat different results (Fig. 6). Handling them under inert atmosphere for the most part avoided the contamination of these spectra with those of U_3O_8 that had been attributed to surface oxidation in the earlier reports. Even for U_3O_7, most of the peaks that might be considered as belonging to U_3O_8, with the exception of the sharp peak around 235 cm^{-1} but including the broad one around 750 cm^{-1} that appears in the three highest oxides, are considerably shifted and exhibit different shapes, although because of their width direct numerical comparison is not necessarily insightful. Corroborating the O XAS, the spectrum of U_4O_9 is not intermediate nor a sum of the UO_2 and U_3O_7 fluorite endpoints. We also note that none of these show the intense uranyl peaks, including the symmetric stretch around 880 cm^{-1} (see Refs. 109 and 110). In this behavior, they recapitulate the U(V) neutron structures, which corroborates the assignment of the U(VI)-oxo moiety to an excitation that is not stimulated by the low-fluence laser used for the Raman spectra. The relative intensities are of interest because, based on the preparation method, it is reasonable to assume that the particles constituting these samples retain their initial morphology and should be similar to each other. Since the Raman cross section correlates directly with the polarizability of the electrons with respect to the vibrational motion, these results indicate that this is increasing substantially as the amount of adventitious O increases, again supporting the idea that there is a significant

modification of the electronic structure even as the fluorite structure is retained.

E. Ultrafast optical pump-probe reflectivity experiments on UO_2, quasiparticle lifetimes

The x-ray measurements have elucidated the behavior of charge inhomogeneities produced by chemical doping. That UO_{2+x} is an insulator[32,111] demonstrates that the charges so induced are pinned by the adventitious O ions that are defects in the lattice and the persistence of the Mott gap, although partly filled Mott insulators, e.g., cuprates, can be exotic metals. The polarons in UO_{2+x} are small and immobile,[54,55] implying large electron-phonon coupling and lattice deformation. We have therefore used optical pumping to induce charge separation and form mobile, polaronic, charge inhomogeneities in UO_2 (see Ref. 62). Although this produces only low and transient carrier concentrations, it has nevertheless been sufficient to tip underdoped cuprates into the superconducting state.[61]

The 3.14-eV excitation has been assigned to a $2U5f^2 \rightarrow U5f^1 + U5f^3$ metal-to-metal charge transfer transition from the occupied $5f$ states of the lower Hubbard band on a U(IV) ion to the unoccupied $5f$ states of the upper Hubbard band on a neighboring U(IV). This initially produces a $U5f^1$-$U5f^3$ excitonic pair, which relaxes within a few dozen psec or less to an intragap state. Optical pumping with the 4.71-eV third harmonic produces the same type of transition across the Hubbard gap but into the $6d$-dominated portion of the upper Hubbard band of the neighboring U(IV). This also relaxes into an intragap state. Probing these intragap states with 1.57-eV pulses shows that the 3.14-eV excitation exhibits two relaxation channels (Fig. 7): a fast electronic one with lifetimes of the order of 10 psec through 1 nsec at, respectively, 300 and 10 K, and a slower lattice one with lifetimes of the order of 1 μsec. That the temperature dependence of the relaxation times of these display virtually identical patterns indicates that the origin of this complicated pattern is a property of the arrangement of atoms rather than of the relaxation mechanism itself. Fluences of 50, 100, and 200 $\mu J \cdot cm^{-2}$ all gave essentially this same pattern. The actual lifetimes, however, were somewhat longer at the higher fluences,[62] which is an indication in this ostensibly defect-free single crystal of self-interaction of the photoinduced quasiparticles. 4.71-eV excitation also shows an asymmetric peak in the lifetimes just below the Neel temperature but, remarkably, none of the other features. Furthermore, the lifetime at this peak is an order of magnitude larger than that with 3.14-eV excitation. The intragap state produced by excitation into the U $6d$ band therefore differs from that resulting from the U $5f$. Since it has μsecs to equilibrate, the barrier between these two distinct quasiparticles must be large in addition to their forming via separate pathways, demonstrating their formation in a nonthermal process that would involve separate paths from their differing initial states.

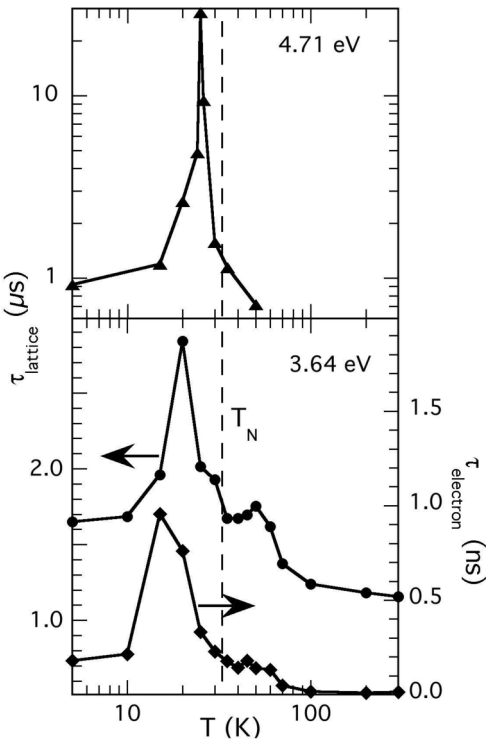

FIG. 7. Photoexcited quasiparticle lifetimes as a function of temperature at listed excitation energies probed at 1.57 eV within the gap. The right hand axis goes with the lowest trace (diamonds), the lower left axis with the middle one (circles), and the upper axis with the upper trace (triangles). The vertical dashed line shows the Neel temperature of the transition to the AFM state in UO_2.

Both the fast and slow lifetimes with 3.14-eV excitation into the U $5f$ band exhibit three distinct regions: (1) around 20–25 K there is a large, asymmetric peak with a width of around 5–10 K that in our previous experiment was obscured because of the coarse temperature intervals; (2) the data points on either side of this peak reveal a flat region that rises slowly to a cusp at 50–60 K that intersects (3) at temperatures $\geqslant$60 K the decrease with power law or exponential-like dependence[62] that is typical of polaronic excitons in transition metal oxides.[112–114] These features clearly do not originate in the small polarons that are the source of the high temperature and persistent low-fluence conductivity.[32,54,55,115]

To interpret these results, we must know whether these complicated lifetime functions originate in properties of the lattice, in which case these findings are relatively mundane, or are signatures of correspondingly complex behavior undergone by the quasiparticles themselves, in which case they are remarkable because of the implications for their self-interaction. The peak can be assigned to the spin-ordering transition that, as described, gives the AFM phase at a Neel temperature of 30.8 K, which is accompanied by 0.014 Å displacements of the ions.[22–24] This is the only transition or other modification of the lattice for UO_2 that has been identified in this temperature region. The lower temperatures of this peak relative to T_N are consistent with the fact that the chemical doping of UO_2 with O to produce UO_{2+x} reduces T_N by up to around 20 K at higher doping levels,[116,117] so disruption of the spins by the quasiparticles could accomplish this as well. In addition, a simple coupling of the quasiparticles to the lattice would be expected, descending from high to low T, to cause a discontinuity in the lifetimes at T_N followed by a continuous modification of the lifetimes proportional to the degree of ordering. Instead, what is observed is a peak, demonstrating that this coupling is indirect. Even more telling

is that the dependence of the lifetimes on temperature differs for the 4.71-eV excitation into the 6*d* states. The two possible causes for this are that the lower fluences for the higher energy excitation result in a quasiparticle concentration below a critical value needed for this pattern to be manifested or that the process that gives the pattern requires excitation into and subsequent prompt relaxation from the U 5*f* state into a specific type of quasiparticle. In either case, the origin of the complicated lifetime pattern is not the response of the quasiparticles to a process occurring in the lattice. These two results are therefore definitive for these features in the lifetimes being coupled not to their UO_2 host but to the properties of the quasiparticles themselves, specifically some type of self-interaction mediated by but separate from the lattice.

This result also assists in interpreting the peak just below T_N that is the most prominent feature in these data. The reduction in temperature below the nominal 30.8 K follows from the free-electron density whose electron-phonon-magnon coupling aids the scattering processes to compete with or inhibit the long-range AFM order. The greater reduction from T_N with higher fluence and presumed higher quasiparticle concentration is consistent with, although not definitive for, this assignment. To reiterate, the reduction of T_N in UO_{2+x}, presumably caused by analogous albeit static defects, is known.[116,117] A peak at T_N instead of a response that is continuous below the AFM region is analogous to what was observed around the superconducting transition in cuprates.[63,72,118] There it was attributed to the coupling of the polaron tunneling to the derivative or gradient of the order parameter for the superconducting transition instead of directly to the transition itself. This interpretation suffices here as well. Of interest is that it implies that the photoinduced quasiparticles are separated from the AFM domains, most likely spatially following from the discussion below. This would cause the lifetimes to be modified only within the relatively narrow fluctuation region of the AFM transition, as is observed, because the spin would permeate into neighboring domains containing the quasiparticles as a result of the fluctuations. Alternatively, it could be a spin ordering or other type of transition of the quasiparticles themselves that is frustrated by competition with another of their intrinsic degrees of freedom, although this seems less likely.

In addition, the difference in the lifetimes between the two excitation energies is also striking. Either the lower concentration of quasiparticles with the lower fluence at 4.71 eV scatters less despite less coherence, or else it corroborates the assignment that these are different kinds of quasiparticles with different properties formed via a different relaxation path or mechanism despite more than adequate time to relax to the lowest intragap state. An analogous direct, nonthermal process could be photoinduced phase transitions.[119] Nonthermal states and differences in the psec relaxations between 3.14- and 4.71-eV pump energies in UO_2 were also found in our very recent photoemission experiments at ambient temperature.[5]

The most intriguing feature of our data is, however, the lifetimes with 5*f* excitation excluding this peak, the combination of the second and third regions. These constitute a flat section at low temperature rising to a cusp at the intersection with the power law region at 50–60 K. This behavior has been associated elsewhere[112] with a gap-opening transition that occurs at the cusp. The transitions that gave this behavior were the formation of a charge density wave (CDW) from a higher symmetry ordered phase and the condensation of disordered quasiparticles into a superconducting phase. Assuming that this cusp in the lifetimes of the photoexcited quasiparticles in UO_2 also signifies their participation in a phase transition, it cannot be a spin-ordering one because this would interact with the AFM phase rather than only with the fluctuations associated with its formation. Because of the peak associated with T_N, it would be difficult to use these data to further characterize the gap, as was done with these other systems, to obtain information on whether this

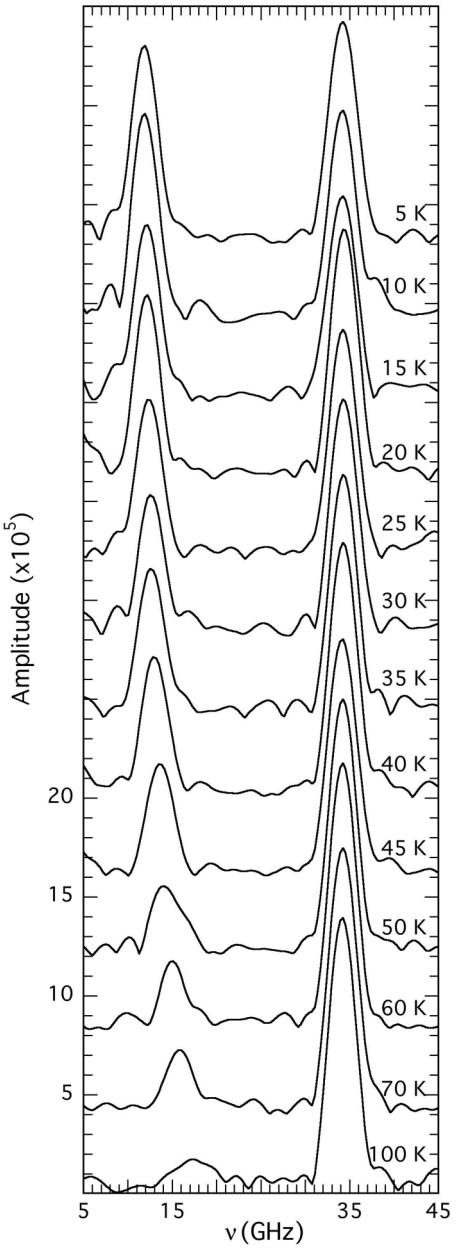

FIG. 8. Phonon spectra generated from ultrafast time-resolved reflectivity spectra at given temperatures. The 34-GHz peak is the collective mode that is the acoustic phonon caused by the shock from the pump pulse; the 12–15 GHz peak is a coherent lattice mode stimulated by the pump pulse.

transition is transition to a CDW, a superconductor, or to an entirely different type and possibly novel type of state. It is also notable that the asymmetry in the peaks with both 3.14- and 4.71-eV excitation gives the appearance of a second cusp. If it is, then there is a second-phase transition of the photoinduced quasiparticles accompanying the AFM one.

F. Ultrafast optical pump-probe reflectivity experiments on UO_2, quasiparticle phonon spectra

Fourier transformation of the time-domain reflectivity data after subtracting the smooth transient portion gives the spectra of the phonons that are coupled to the excitation because their stimulation by the pump pulse makes them coherent over the area of the subsequent probe pulse (Fig. 3). This process must give the acoustic phonon stimulated by the impulse of the pump that always occurs in a pump-probe experiment.[120,121] For UO_2, this is the peak at 33 GHz whose position is invariant over the entire temperature range (Fig. 8). Other phonons whose behaviors are time dependent are therefore used to track the property of interest that is stimulated by the pump pulse. This has most typically been the recovery of a structure or species that was disrupted by the pump.[121,122] Furthermore, these should be collective rather than local modes since the latter would rapidly lose coherence over the large area of the probe beam and would not give a signal.

In contrast, in this measurement on UO_2 the phonon and the species or structure in which it originates are created by the photoexcitation and subsequently decay with time. This is the second peak around 12 GHz ($\sim$60 μV) at 5 K that is thus assigned to the photoinduced quasiparticles. This phonon hardens continuously over the entire temperature range. Although from 5 to 50 K it resembles the 33 GHz peak in being highly symmetric, as the temperature continues to be elevated this peak first becomes noticeably asymmetric on the high frequency side, and then this asymmetry evolves into multiple peaks even as the principal peak continues to harden. Although its amplitude decreases monotonically with temperature through 50 K to approximately one-third its original value, this trend is broken for 50, 60, and 70 K where it is almost constant. This trend is clearer when plotting the area of this feature that includes the higher frequency peaks that have split off from the primary one (Fig. 9). A distinct break in the slope of the areas found by curve fits with one or more Gaussians that diminish with increasing temperature is observed at 50 K, whereas the amplitudes and areas of the acoustic phonon peak increase slowly and continuously while flattening out at higher temperatures. The temperature dependence of areas, frequencies, and shapes of this phonon are therefore the same as for the lifetimes in displaying two distinct trends that change at 50–60 K. The simplest explanation is that this phonon is a signature of the self-organized quasiparticle phase whose formation is signified by the cusp at 50–60 K.

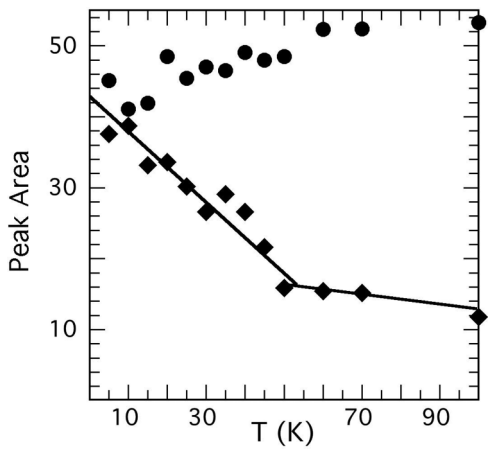

FIG. 9. Areas of the peaks from the collective mode at 34 GHz (circles) and the coherent lattice mode at 12–15 GHz (diamonds). The lines are guides.

Although we have not yet measured the energy of the gap produced in the 50–60 K transition,[121] some insight is obtained from estimating the composition of the excited state. Although there is a wide range of optical densities reported for UO_2, using the 0.1/nm at 2.0 eV value from Siekhaus[123] rather than the ones from Chen[124] that vary only slightly with film thickness or the older ones from Griffiths[125] that correspond to 0.001/nm or Meek[126] that give around 0.007 at 3.2 eV, we calculate approximately 0.5 photons absorbed per nm^3 in the top layers of the material. This corresponds to 2% of the U sites associated with hole polarons. The accompanying change in reflectivity would be 0.025 per polaron. For comparison, this change in $TbTe_3$ that must have involved a much greater number of polarons was almost 10 times as large.[122] The changes in reflectivity are therefore consistent with the differences in the underlying physics. We believe that this is sufficiently large for the quasiparticles to aggregate into observable domains within the host UO_2 of a separate phase, especially if its structure includes, in addition to the holes, U(IV) sites and possibly the electron polarons. However, at this concentration, these condensate domains would occupy only a fraction of the volume within the UO_2 host, as implied by its interaction with the AFM transition.

G. Ultrafast time-resolved optical pump-terahertz probe measurements of UO_2

Optical pump-terahertz probe experiments complement the pure optical ones by identifying and characterizing very low energy excitations. These include, e.g., collective phonons at energies below the conventional vibrational region[127] and, for complicated molecules, local modes as peaks on a smooth, monotonically increasing background down to and below 1 THz. In addition, terahertz spectroscopy probes conductivity in the form of plasmons and other freely mobile carriers but also superconductivity as well as polaronic and spin-coupled activated transport associated with a lattice distortion. It can therefore be used to directly identify and characterize carriers produced by optical pumping. UO_2 does not possess phonons of this type[19–21,107,108,128] so that its static, unexcited spectra are featureless in this region, curving upward with increasing frequency (Fig. 10). The real part of the complex dielectric function, ε_r, increases with increasing temperature. Both of these results are consistent with a wide band-gap semiconductor[125,126,129,130] with small polarons,[54] as has been observed in previous slow photoexcitation experiments.[115] ε_i is relatively temperature independent, which is unusual for

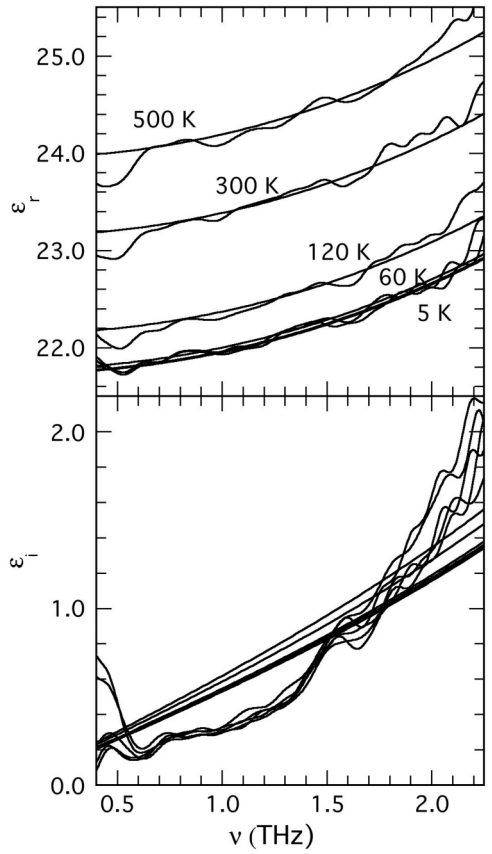

FIG. 10. Terahertz time-domain spectra of ground state UO_2 at indicated temperatures. Thinner lines are fits to data using the Lorentz oscillator model.

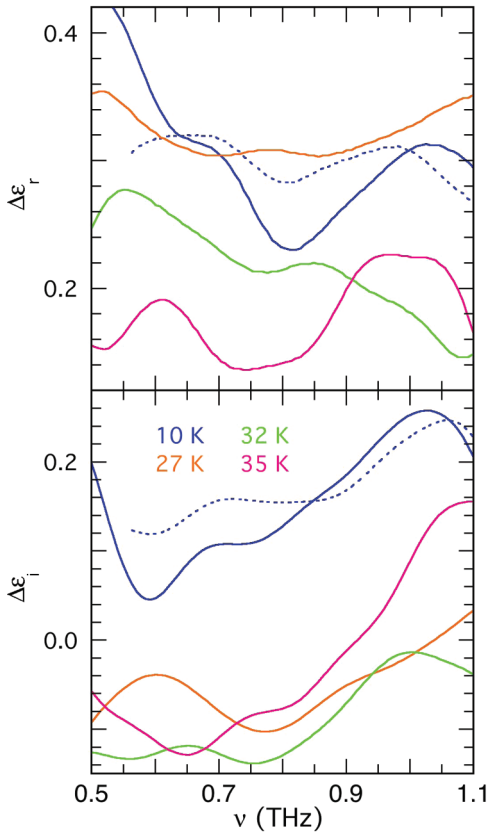

FIG. 11. (Color online) Terahertz time-domain difference spectra of photoexcited (3.14 eV) minus ground state UO_2 at indicated temperatures. The dotted traces at 10 K are from a second measurement and provide an indication of the reproducibility of these results.

these types of systems. The upward curvatures of the complex dielectric function, ε_r and ε_i, are well fit with a Lorentz oscillator, although the actual slope in ε_i may be larger than this function, confirming that this is normal vibrational behavior.

The properties of the photoexcited state at low temperatures were examined by exciting at 3.11 eV and obtaining the TTDS spectra 33 psec afterwards, then subtracting the spectra from the ground state system to obtain the difference spectra, $\Delta\varepsilon_r$ and $\Delta\varepsilon_i$. Our pump-probe reflectivity measurements show that this interval is sufficient to relax from the initial excited state into the long-lived intragap states characterized in those experiments. $\Delta\varepsilon_r$ and $\Delta\varepsilon_i$ should therefore give the spectra of the intragap quasiparticles. At this crystal thickness and at these fluences, the optical density of the excited state is only a few percent of the total, unlike other systems such as semiconductors, so that the signal is relatively weak and reliable data were obtained only over a limited region (Fig. 11). The 10 K measurement that was performed twice independently gives an indication of the reproducibility of the results. Despite this weak signal, some important trends can be discerned.

No specific, reproducible, peak-like features are observed, so there are neither phonons nor local vibrational modes from the quasiparticle states that give signals above the noise level unless they are specific to a single temperature. $\Delta\varepsilon_r$ and $\Delta\varepsilon_i$ both exhibit increases as T is lowered, although for $\Delta\varepsilon_r$ this may be continuous until it saturates at 27 K while only increasing between 27 and 10 K in $\Delta\varepsilon_i$, signifying an increase in the conductivity that is antithetical to conventional small polaron behavior. $\Delta\varepsilon_i$ therefore does not respond to the AFM transition, and if the increase in $\Delta\varepsilon_r$ is associated with it then it would be expected that it would continue to grow as the temperature is further lowered. Although this behavior could be consistent with the carrier lifetimes in a photoexcited system, in photoexcited Si the highest values occur at intermediate temperatures and are significantly lower in this range.[127] The initial increase in photoexcited Si as the temperature is lowered is because of longer carrier lifetimes; the subsequent rollover occurs because, even with a large polaron with a small lattice distortion, the motion of the charges is still hopping, is still thermally activated, and will eventually freeze out as the temperature continues to decrease. In addition, the slopes of both ε_r and ε_i with increasing energy are negative in photoexcited Si. $\Delta\varepsilon_r$ has been found to increase continuously as the temperature is decreased in manganites, but this was attributed to the coupling of the conductivity to the overall magnetization[131] that is irrelevant to UO_2 because the quasiparticles do not interact directly with the AFM phase. The most germane systems are therefore superconductors. These give different responses depending on whether their gap is within or above the terahertz spectrum, corresponding to, respectively, more conventional materials and cuprates. BCS theory predicts that whereas the slope of ε_i remains negative, ε_r will increase sharply from a discontinuity at the gap, with

ε_r below the gap decreasing as T approaches T_c but becoming flatter at lower temperatures.[132,133] More recent experiments on cuprates[134,135] have elaborated on this, showing that ε_r is the signal from isolated quasiparticles, whereas ε_i is the absorbance from the condensate, and below the gap they both tend to go as $1/\omega$, more steeply as the temperature is decreased.[136] These spectra for photoexcited UO_2 appear to have a flat or possibly descending $\Delta\varepsilon_r$, an increasing $\Delta\varepsilon_i$, an increase in both at the lowest temperatures even across this narrow range, and the possibility for $\Delta\varepsilon_i$ that the excitation causes a decrease in absorbance at low frequencies at the higher temperatures. The TTDS of photoexcited UO_2 therefore does not match the behavior of any of these other systems. This last result, however, does point to transient photoinduced conductivity with no or only a minimal (<10 K) barrier to the carrier motion. The total conductivity would also be consistent with an increased concentration of quasiparticles as the temperature is decreased from 27 to 10 K that condense rather than remaining separated.

Another unusual or possibly unique characteristic of this system is the mechanism of this DC conductivity in the context of the quasiparticle aggregation and self-organization into a distinct phase. The conductivity expected from the normal small polarons would be much less than that observed, so that it must be occurring within this domain containing the quasiparticles. The total volume of material occupied by this phase, however, must be a relatively small fraction because the optical pumping does not come close to saturating it. This implies that in addition to the lifetime of the individual quasiparticles and their possible condensation at the lowest temperatures, another crucial parameter is the duration of their percolation.

III. DISCUSSION

We have repeated on samples from the same batches of UO_2, U_4O_9, and U_3O_7 both the previously reported neutron scattering[41] and EXAFS results[57] and added the x-ray pdf. These give the ostensible contradiction found in the literature, with the neutrons finding a much smaller lattice distortion than the x rays in the mixed valence UO_{2+x} compounds; however, we can now reconcile this within the framework of a lattice instability involving polaron tunneling in U_4O_9 and U_3O_7. The conceptual basis for this intrinsic dynamics in UO_{2+x} was originally found in cuprate superconductors[63,65,66,72,74,118] and subsequently became a characteristic of functionally layered materials in which nonstoichiometric chemical substitution and subsequent mixed-valence character produce atomic-scale spin and charge inhomogeneities. Exotic metallic behavior is a property of Mott-Hubbard systems with intermediate electron-phonon coupling, occurring when the doping is sufficient enough to effect the transition to the Fermi-liquid state. Prior to saturation that gives another insulating phase, the strong Coulomb repulsion in the intermediate doping systems causes self-organization and phase separation of the mobile charges that results in their condensing into structures encompassing multiple length scales, e.g., stripes,[65,68,69,137–141] fractals,[142] etc.[143,144]

The tunneling between degenerate configurations of the atoms inherent to the intermediate electron-phonon coupling regime and anharmonicity of these polarons causes the determination of their structures to be sensitive to the time and energy scale domains of the probe[63–67,74] via the dynamic structure factor, $\int_0^{\omega_T} d\omega S(r,\omega)$. Slow, low-energy probes, e.g., neutrons, give the average distribution over the nodeless ground vibrational state. Fast, high energy ones, e.g., x rays, excite the system by scattering inelastically and image the double-well potential in which the tunneling occurs.[67,73,74] Essential to this process, however, is that the distortion of both the lattice and electronic structure are relatively small so that the barrier is low and narrow enough for the O ions to tunnel through it.[67,72,73] The coupling of the motions of the charges and the atoms places the affected electrons in the nonadiabatic regime,[72] negating the Born-Oppenheimer approximation[67] and creating the possibility of the potential energy surfaces of the ground and excited electronic states interacting to form a conic section. The intersection of the ground U(V) and excited U(VI)-oxo state potentials not in the usual cusp but smoothly and continuously in such a conic section would be a consequence of the uniquely flat potential of the U(VI)-O bond with respect to its various environments, as described in the Introduction. Such conic sections have been associated with unusual dynamical properties in small molecules[145] but have not yet been identified or even proposed in condensed materials and would contribute to the unusual properties found in these experiments and discussed in the remainder of this report.

As described in the Introduction, intrinsic dynamics have already been reported in UO_2 in the form of dynamic Jahn-Teller distortions.[9,15,17,19] These are, however, not associated with the phenomena we report here. The softening of the c_{44} elastic constant[19,128] and other neutron and x-ray scattering anomalies[146] have been shown to be associated with the continuous ordering of the individual magnetic moments to give the AFM phase. The 0.014 Å displacements of the O ions[22–24] are indicative of a role for the lattice and magnon-phonon interactions[11] and specifically multipolar superexchange interactions.[21] However, they pertain strictly to undoped UO_2 and therefore do not include mixed valence nor charge transfer. Moreover, the order of the 10-meV energy scale on which these Jahn-Teller excitations occur is two orders of magnitude lower than the 1-eV energy of the intragap states and almost two orders of magnitude higher than the associated 60-μV coherent phonon. One relevant point is that these other studies are conclusive in demonstrating that the only known phase transition in this range is the AFM one at 30.8 K with no others that could give the cusp at 50–60 K in the optical measurements. A second point is that these measurements and associated calculations[10,15–17,147] did not show any significant perturbation of the electronic structure that might be associated with these small lattice distortions in UO_2, leaving the intrinsic dispersion[4,5,71] and inferred covalence of the U-O bond as the initial departure from purely ionic behavior and small polarons.

Another property that has been observed in intermediate doping Mott-Hubbard systems is a direct coupling between phonons and charge that promotes dynamical charge transfer between, e.g., Cu and O.[148] Although UO_{2+x} exhibits these characteristics, such descriptions of dynamical structures[67,72] are not applicable because the properties of the dynamical

polaron in UO_{2+x} are much more extreme than those observed in cuprates and related materials. Not only is the 0.6 Å difference between the U-O distance in UO_2 and the measured U(VI)-oxo-type distance impossibly large for this type of tunneling—the 0.13 Å distance in cuprates[65,72,118] was already considered marginal—but the widths of the U-U and a number of other pair distributions are much wider in the dynamic rather than in the elastic measurements, whereas this original mechanism dictates that they be the same. In addition, although in cuprates only the two identical O ions around a particular Cu were in motion, in UO_{2+x} the number of atoms involved in this transformation from a symmetric U(V) to the U(VI)-oxo species of the cluster is much greater and more extensive and also requires a total alteration of the geometry and associated electronic structure. Finally, the fluctuation region characterized by a variable structure because the barrier separating the two endpoints flattens, which in cuprates[63–65] is only a few K wide and centered on the superconducting transition, is, based on the EXAFS of UO_{2+x} at 30–200 K, enormously wide and not coupled to a known phase change in UO_{2+x}.

These inconsistencies with the simple tunneling polaron mechanism mandate a novel process in UO_{2+x}. The 1.7 Å U-O distance indicates that the excitation is electronic instead of vibronic with a structure factor, $\int_o^{\varepsilon_T} d\varepsilon S(r,\varepsilon)$, that originates in the disproportionation 2 U(V) $\leftrightarrow$ U(IV) + U(VI)-oxo that is facilitated by the unusual juxtaposition of the U(IV/V) and U(VI) potential surfaces and resulting lattice instability of UO_{2+x}. One possibility subsequent to the formation of U(VI)-oxo sites is a local rotation of its oxo groups around a single U(VI) ion, maintaining the structure but switching its orientation relative to the crystal axes. However, the most likely mechanism that extends the one-dimensional radial information to a more comprehensive picture is derived from the oxidation of bulk-cubic UO_2 to layered U_3O_8 (see Refs. 35 and 43). This involves transformation of the (111) U planes of UO_2 that are separated by 3.13 Å into the (001) U-O_x planes of U_3O_8 and α-UO_3 that have a spacing of 4.16 Å [Fig. 12(a) and 12(b)]. A contraction of the [111]-oriented U-O bonds concomitant with a displacement in the opposite direction of the neighboring plane containing the other three U ions composing the tetrahedral O site of UO_2 increases these other U-O distances; an expansion of the interplanar distance by only 0.68 Å coupled to the formation of a 1.7 Å uranyl-type bond increases these U-O distances to 3.01 Å, which is essentially nonbonding. This includes the a-b displacement between neighboring U planes that gives them an -a-b-c-a- stacking pattern in UO_2 that increases the U-O distances to neighboring U sites relative to U_3O_8 where the U ions form a chain.

The U positions within these planes are almost identical in the UO_2 and UO_3 structures [Fig. 12(c)]. Only minimal or negligible U displacements are therefore required in this reaction, and the amount of epitaxial strain is also quite low. Smaller displacements of the other O ions complete the formation of the (001) UO_x planes. The additional O ions in the cuboctahedra or quad-interstitials of U_4O_9 or the U_4O_9-type clusters in UO_{2+x} would facilitate this by shifting to give the second O ion of the preferred transdioxo configuration, completing the transition between the more spherical U(IV/V) local geometry

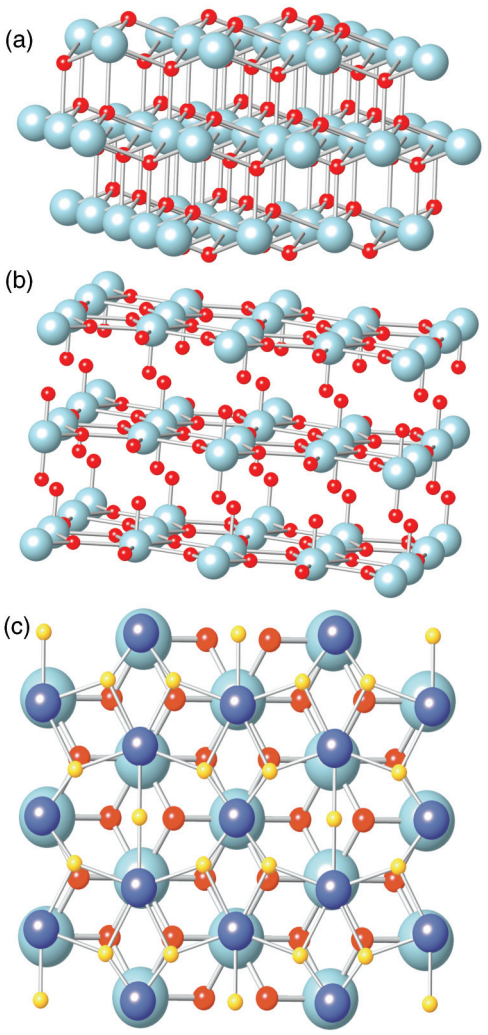

FIG. 12. (Color) (a) UO_2 viewed along the (111) U planes: U atoms are blue; O are red or yellow. The separation between these planes is 3.14 Å. (b) α-UO_3 viewed along the (001) planes that are separated by 4.16 Å. This structure has the U_3O_8 composition, in αUO_3 the c-oriented -U-O–U–O-U- chains are broken by the removal of $\frac{1}{9}$ of the U ions. (c) Overlay of (111) plane of UO_2 (under) and, on exactly the same scale, (001) plane of α-UO_3 (over) showing relative positions of atoms.

favored by these conformations to the layered structure with oblate trans-dioxo moieties that would give an α-UO_3-like configuration.

A single uranyl defect in the fluorite lattice would be highly strained, and the energy of its formation is correspondingly high. This mechanism would lower the formation energy substantially because instead of the tunneling being a local mode, it occurs as a synchronized excitation that would be a collective, dynamical, charge transfer-coupled, Peierls distortion throughout the O-enriched domain. The broadening and enhanced overlap of the electronic states we observe would also assist in reducing the barrier and facilitating the tunneling. A [111]-oriented acoustic phonon that dynamically alters the interplanar spacing would therefore cause the relative stability of U(IV/V) and (VI)-oxo configurations to oscillate in tandem with the motions of the planes and easily provide an impetus

for such a concerted excitation. This phonon also makes the motions of the atoms and charges coherent throughout the domain in which it occurs.

We now address the behavior of the transient photoinduced polaronic quasiparticles. In a lattice free of defects, these provide the opportunity to explore the behavior of charge inhomogeneities that may move freely through the material, assuming that the associated deformation of the lattice is small corresponding to intermediate electron-phonon coupling or if polaron transport is facilitated by some other mechanism. The temperature dependence of the lifetimes strongly implies that these particles aggregate, self-organize, and condense into a quantum phase analogous to the clustering and phase separation of adventitious O in UO_{2+x} with its chemically induced charge inhomogeneities. This quantum phase undergoes at least one and possibly two transitions: a higher temperature gap opening one that is completely separated from the AFM transition and only occurs with excitation into the $5f$-dominated portion of the upper Hubbard band and a possible second transition at lower temperature overlapping with the AFM transition, which could be coupled to the spin ordering including the depression of T_N by the quasiparticles and may occur with both excitation channels. The first phase has a second signature in addition to the lifetimes, a 12–15 GHz phonon. Within this scenario of condensation being the most plausible explanation of these data, it is nevertheless useful to consider the intrinsic phonon associated with the ground state CDW in $TbTe_3$ (see Ref. 122). This CDW is disrupted by the pump so that the signature of its restoration is the development of these intrinsic phonons that soften as their ordering and size increase with time. In contrast, this phonon in UO_2 that is associated with excitation instead of being a property of the ground state dissipates with time and hardens and broadens with increased temperature as the quasiparticle lifetime diminishes.

This phonon does not occur in the ground state phonon DOS of UO_2 (see Refs. 14, 21, 128, and 149). Combined with its correlation with the lifetime results, this demonstrates that it is created by the photoexcitation. The single Gaussian peak in the phonon spectrum below 50 K therefore belongs to the phase created by the gap-opening transition. The change in the pattern above 50–60 K could indicate some type of precursor activity or another ordered phase obscured by the faster quasiparticle relaxation above this temperature. The presence of this coherent mode thus necessitates an ordered structure with a domain size sufficient to support a coherent oscillation of the ions within at least a several nm extent, comparable to the O-enriched domains of UO_{2+x} at low x.[7,34,38,39,46,53,56] These are the same domains where the U(V) sites cluster that are consequently the location of the intrinsic dynamics because of the coherent 2 U(V) $\leftrightarrow$ U(IV) + U(VI)-oxo disproportionation. The simplest explanation is that this same process occurs with photoexcitation, the diffusion, aggregation, and self-organization of the U(V) into separate, ordered domains that are subsequently susceptible to this charge-transfer excitation that results in coherence and condensation. This raises the question of how it occurs just as or perhaps even more easily in the absence of extra O ions and in the presence of the U(III) ions that are the partners to the U(V) from the metal-to-metal charge transfer. These will be addressed with further examination. Certainly the U(III) to some extent must be collocated with the U(V) to maintain charge balance or else the domain size would be extremely limited. Alternatively, maintaining charge balance could also be facilitated if the U(VI)-oxo domains were two- rather than three-dimensional. If the U(V) ions are all involved in the excitation, the U(III) may even be the source of the optically induced conductivity.

The low frequency of the phonon implies either correspondingly slow tunneling of a small polaron or a collective motion that could include tunneling of a large number of atoms such as the proposed phase or condensate. If the latter occurs, then this phonon could well be the tunneling excitation itself. The structural fluctuations in the U-O distribution that we observe in UO_{2+x} as low as between 30 and 100 K place an upper bound of 9 meV (and possibly much lower) on the tunneling of the U(VI)-oxo polarons, definitely favoring the latter interpretation since such slow tunneling for a single particle necessitates a large barrier. The complexity of the temperature dependence at and above the transition suggests the formation of small aggregates as precursors of the ordered phase, which would be more consistent with a condensation type of transition. This raises the question of the nature of the gap. A CDW would not exhibit the conductivity shown by the TTDS results. Before suggesting that it is superconducting, however, what must be considered is that this conductivity is unlikely to be a homogeneous property because of the low-carrier concentration. Insofar as the initial state has no low energy carriers and photoexcitation in cuprates is barely able to induce enough to cross from just below to just above the superconducting transition,[61] it is remarkable that the optical pumping creates enough quasiparticles to give these properties. They almost certainly occur in domains within the host UO_2, caused by the clustering of the U(V) ions. In this case, the conductivity observed in the TTDS depends on percolation as well as carriers, and the increase as the temperature is lowered could be from conventional conduction and longer range percolation as well as increased carrier lifetimes.

The increase in the TTDS absorption between 30 and 10 K makes another important connection with the EXAFS. The latter indicates that the barrier to local rearrangement of the O ions in UO_{2+x} is very low. Since the O lattice defects pin the charge defects or inhomogeneities in UO_{2+x}, this would be expected to only affect the polarizability that might contribute to the ac conductivity. This same facilitated motion is obviously crucial in DC conductivity as well, which in the absence of lattice defects would result from the transport of the polaronic quasiparticles through extended, connected domains. The optical pump-terahertz probe measurements meet these conditions. The implied increase in dc conductivity with the optically induced carriers at low temperature, if it is not indicative of superconductivity, is therefore consistent with a minimal barrier for O motion between its sites that give the distinct U(IV/V) and U(VI) geometries in UO_{2+x} whose unusually or uniquely low value would point to a comparably interesting phenomenon. In addition, although not indicative, the increase in ε_r followed by the increase in ε_i as the temperature is lowered further is what would be expected for condensate formation from isolated quasiparticles.

The sum of these unusual and unique properties observed in this extensive set of experiments indicate that UO_{2+x} most

likely contains a novel form of quantum matter. We propose that the aggregation of the U(V) sites and the subsequent collective, charge transfer, Peierls distortion might stimulate a Bose-type condensation of the polaronic quasiparticles, albeit one where the coherence results from a synchronous excitation of the particles rather than lowering the energy of all of them into their ground state. This mechanism provides an explanation for many of the properties that are difficult or impossible to explain using familiar mechanisms. The dynamical displacements of the ions that are far too large for normal tunneling would occur easily within the superfluid droplets of such a condensate.[150] It would also produce the fluctuations in the U-O distribution observed at >150 K, albeit while raising the question of why this BEC-like behavior is occurring at such high temperatures in a condensate of polarons in a crystal lattice. A polaronic condensate would be consistent with, and also provides a mechanism for, our ultrafast optical pump-probe measurements that show aggregation and ordering of the photoinduced, intragap quasiparticles and their participation in a separate gap-opening phase transition. Multiple phases, including Mott insulating as well as Bose superfluid ones, were predicted for a Bose-Hubbard system consisting of quasiparticles in a periodic lattice with onsite repulsion between them, a "Bose-(Einstein-)Hubbard" condensate.[75,76] In addition, the stabilization that these systems display when consisting of holons and doublons relative to fermions that stabilizes U(VI) would,[151] in tandem with the flat U-O potentials, help explain the low energy of the disproportionation excitation that converts the U(V) into U(IV) and the U(VI)-oxo moieties.

A Bose-Einstein or Bose-Hubbard condensate or an alternative phenomenon that would give similar properties that contain charge and spin degrees of freedom within condensed material through ambient temperature, if confirmed, would have tremendous scientific and technological implications. The next step is to find a way to induce a static concentration of charges in crystalline UO_2. Synthesis of a layered material with functionally distinct conductive and charge reservoir domains is nontrivial because the fluorite structure of UO_2 and the cubic or spherical geometry of U(IV) are not conducive to layered structures. A successful strategy might therefore involve templating UO_2 onto a material that does prefer layers. We note that, in an odd coincidence, the (111) plane of UO_2 fits quite well to the (001) CuO_2 plane in cuprates.

ACKNOWLEDGMENTS

This work was supported at Los Alamos by the Division of Chemical Sciences, Geosciences, and Biosciences, Office of Basic Energy Sciences, U.S. Department of Energy under the Heavy Element Chemistry and Material Science and Engineering Programs at LANL, and the Los Alamos Laboratory Directed Research and Development Program. Portions of this research were carried out at the Stanford Synchrotron Radiation Lightsource, the Lujan Neutron Scattering Center, the Advanced Photon Source, and at the Center for Integrated Nanotechnologies, all of which are national user facilities supported by the U.S. Department of Energy, Office of Basic Energy Sciences, and at the Environmental Molecular Science Laboratory, a national scientific user facility sponsored by the Department of Energy's Office of Biological and Environmental Research and located at Pacific Northwest National Laboratory. Los Alamos National Laboratory is operated by Los Alamos National Security, LLC, for the National Nuclear Security Administration of U.S. Department of Energy under Contract No. DE- AC52-06NA25396. PNC/XOR facilities at the Advanced Photon Source, and research at these facilities, are supported by the U.S. Department of Energy-Basic Energy Sciences, a Major Resources Support grant from NSERC, the University of Washington, Simon Fraser University, and the Advanced Photon Source.

*Corresponding author: conradson@lanl.gov
†Current address: SUNY Albany, Albany, New York 12222, USA.
‡Current address: Stanford University, Stanford, California 94305, USA.
§Current address: Oak Ridge National Laboratory, Oak Ridge, Tennessee 37831, USA.

[1]P. C. Burns, R. C. Ewing, and A. Navrotsky, Science **335**, 1184 (2012).
[2]J. Schoenes, J. Chem. Soc., Faraday Trans. 2 **83**, 1205 (1987).
[3]S. W. Yu, J. G. Tobin, J. C. Crowhurst, S. Sharma, J. K. Dewhurst, P. Olalde Velasco, W. L. Yang, and W. J. Siekhaus, Phys. Rev. B **83**, 165102 (2011).
[4]X.-D. Wen, R. L. Martin, L. E. Roy, G. E. Scuseria, S. P. Rudin, E. R. Batista, T. M. McCleskey, B. L. Scott, E. Bauer, J. J. Joyce, and T. Durakiewicz, J. Chem. Phys. **137**, 154707 (2012).
[5]S. M. Gilbertson, T. Durakiewicz, G. L. Dakovski, L. Yinwan, J. X. Zhu, S. D. Conradson, S. A. Trugman, and G. Rodriguez, Phys. Rev. Lett. (to be published).
[6]W. T. Thompson, B. J. Lewis, E. C. Corcoran, M. H. Kaye, S. J. White, F. Akbari, Z. He, R. Verrall, J. D. Higgs, D. M. Thompson, T. M. Besmann, and S. C. Vogel, Int. J. Mater. Res. **98**, 1004 (2007).
[7]D. A. Andersson, G. Baldinozzi, L. Desgranges, D. R. Conradson, and S. D. Conradson, Inorg. Chem. **52**, 2769 (2013).
[8]K. E. Knope and L. Soderholm, Chem. Rev. **113**, 944 (2013).
[9]S. Kern, C. K. Loong, and G. H. Lander, Physica B & C **136**, 403 (1986).
[10]R. Osborn, A. D. Taylor, Z. A. Bowden, M. A. Hackett, W. Hayes, M. T. Hutchings, G. Amoretti, R. Caciuffo, A. Blaise, and J. M. Fournier, J. Phys. C Solid State **21**, L931 (1988).
[11]R. Caciuffo, G. Amoretti, P. Santini, G. H. Lander, J. Kulda, and P. D. Du Plessis, Phys. Rev. B **59**, 13892 (1999).
[12]V. S. Mironov, L. F. Chibotaru, and A. Ceulemans, in *Advances in Quantum Chemistry*, Vol. 44: Manifestations of Vibronic Coupling in Chemistry and Physics, edited by A. Ceulemans, L. Chibotaru, and E. Kryachko (Elsevier, Amsterdam, 2003), pp. 599–616.
[13]B. Dorado, G. Jomard, M. Freyss, and M. Bertolus, Phys. Rev. B **82**, 035114 (2010).
[14]J. Schoenes, Phys. Rep. **63**, 301 (1980).
[15]S. Kern, C. K. Loong, and G. H. Lander, Phys. Rev. B **32**, 3051 (1985).
[16]Z. Gajek, M. P. Lahalle, J. C. Krupa, and J. Mulak, J. Less-Common Met. **139**, 351 (1988).

[17]G. Amoretti, A. Blaise, R. Caciuffo, J. M. Fournier, M. T. Hutchings, R. Osborn, and A. D. Taylor, Phys. Rev. B **40**, 1856 (1989).
[18]O. G. Brandt and C. T. Walker, Phys. Rev. **170**, 528 (1968).
[19]P. D. V. Duplessis, G. H. Lander, A. M. Strydom, and B. Fak, Physica B **180**, 321 (1992).
[20]T. Livneh, J. Phys.: Condens. Matter **20**, 085202 (2008).
[21]R. Caciuffo, P. Santini, S. Carretta, G. Amoretti, A. Hiess, N. Magnani, L. P. Regnault, and G. H. Lander, Phys. Rev. B **84**, 104409 (2011).
[22]B. T. M. Willis and R. I. Taylor, Phys. Lett. **17**, 188 (1965).
[23]B. C. Frazer, G. Shirane, D. E. Cox, and C. E. Olsen, Phys. Rev. **140**, 1448 (1965).
[24]J. Faber, G. H. Lander, and B. R. Cooper, Phys. Rev. Lett. **35**, 1770 (1975).
[25]S. Van den Berghe, M. Verwerft, J. P. Laval, B. Gaudreau, P. G. Allen, and A. Van Wyngarden, J. Solid State Chem. **166**, 320 (2002).
[26]R. B. King, Chem. Mater. **14**, 3628 (2002).
[27]P. G. Allen, D. K. Shuh, J. J. Bucher, N. M. Edelstein, C. E. A. Palmer, R. J. Silva, S. N. Nguyen, L. N. Marquez, and E. A. Hudson, Radiochim. Acta **75**, 47 (1996).
[28]P. G. Dickens and A. V. Powell, J. Mater. Chem. **1**, 137 (1991).
[29]H. M. Rietveld, Acta Crystallogr. **20**, 508 (1966).
[30]C. Greaves and B. E. F. Fender, Acta Crystallogr. B **28**, 3609 (1972).
[31]M. T. Weller, P. G. Dickens, and D. J. Penny, Polyhedron **7**, 243 (1988).
[32]T. R. Griffiths, V. S. A. Hubbard, and M. J. Davies, Inorg. Chim. Acta **225**, 305 (1994).
[33]R. G. Haire and L. Eyring, in *Handbook on the Physics and Chemistry of the Rare Earths*, edited by K. A. Gschneidner, Jr., L. Eyring, G. R. Choppin, and G. H. Lander (Elsevier Science, B.V., New York, 1994), p. 413.
[34]G. C. Allen and P. A. Tempest, Proc. R. Soc. London Ser. A **406**, 325 (1986).
[35]G. C. Allen and N. R. Holmes, J. Nucl. Mater. **223**, 231 (1995).
[36]B. T. M. Willis, Solid State Comm. **2**, 23 (1964).
[37]B. T. M. Willis, J. Chem. Soc., Faraday Trans. 2 **83**, 1073 (1987).
[38]F. Garrido, R. M. Ibberson, L. Nowicki, and B. T. M. Willis, J. Nucl. Mater. **322**, 87 (2003).
[39]L. Nowicki, F. Garrido, A. Turos, and L. Thome, J. Phys. Chem. Solids **61**, 1789 (2000).
[40]R. I. Cooper and B. T. M. Willis, Acta Crystallogr. A **60**, 322 (2004).
[41]F. Garrido, A. C. Hannon, R. M. Ibberson, L. Nowicki, and B. T. M. Willis, Inorg. Chem. **45**, 8408 (2006).
[42]F. Garrido, L. Nowicki, and L. Thome, Phys. Rev. B **74**, 184114 (2006).
[43]L. Desgranges, G. Badinozzi, D. Simeone, and H. E. Fischer, Inorg. Chem. **50**, 6146 (2011).
[44]G. C. Allen, P. A. Tempest, and J. W. Tyler, J. Chem. Soc. Farad. T. 1 **83**, 925 (1987).
[45]K. Naito, T. Tsuji, and T. Matsui, J. Radioanal. Nucl. Chem.-Artic. **143**, 221 (1990).
[46]A. D. Murray and B. T. M. Willis, J. Solid State Chem. **84**, 52 (1990).
[47]N. C. Popa and B. T. M. Willis, Acta Crystallogr. A **60**, 318 (2004).
[48]H. M. He and D. Shoesmith, PhysChemChemPhys **12**, 8108 (2010).
[49]D. J. M. Bevan, I. E. Grey, and B. T. M. Willis, J. Solid State Chem. **61**, 1 (1986).
[50]P. A. Tempest, P. M. Tucker, and J. W. Tyler, J. Nucl. Mater. **151**, 251 (1988).
[51]H. Y. Geng, Y. Chen, Y. Kaneta, and M. Kinoshita, Phys. Rev. B **77**, 180101 (2008).
[52]D. A. Andersson, J. Lezama, B. P. Uberuaga, C. Deo, and S. D. Conradson, Phys. Rev. B **79**, 024110 (2009).
[53]D. A. Andersson, F. J. Espinosa-Faller, B. P. Uberuaga, and S. D. Conradson, J. Chem Phys. **136**, 234702 (2012).
[54]J. M. Casado, J. H. Harding, and G. J. Hyland, J. Phys.-Condens. Matter **6**, 4685 (1994).
[55]P. Ruello, K. D. Becker, K. Ullrich, L. Desgranges, C. Petot, and G. Petot-Ervas, J. Nucl. Mater. **328**, 46 (2004).
[56]S. D. Conradson, B. D. Begg, D. L. Clark, C. den Auwer, M. Ding, P. K. Dorhout, F. J. Espinosa-Faller, P. L. Gordon, R. G. Haire, N. J. Hess, R. F. Hess, D. W. Keogh, G. H. Lander, D. Manara, L. A. Morales, M. P. Neu, P. Paviet-Hartmann, J. Rebizant, V. V. Rondinella, W. Runde, C. D. Tait, D. K. Veirs, P. M. Villella, and F. Wastin, J. Solid State Chem. **178**, 521 (2005).
[57]S. D. Conradson, D. Manara, F. Wastin, D. L. Clark, G. H. Lander, L. A. Morales, J. Rebizant, and V. V. Rondinella, Inorg. Chem. **43**, 6922 (2004).
[58]E. Schofield, A. Mehta, S. Webb, K. U. Ulrich, D. E. Giammar, J. O. Sharp, H. Veeramani, R. Bernier-Latmani, S. Conradson, D. Clark, and J. R. Bargar, Geochim. Cosmochim. Acta **72**, A838 (2008).
[59]S. D. Conradson, B. D. Begg, D. L. Clark, C. Den Auwer, F. J. Espinosa-Faller, P. L. Gordon, N. J. Hess, R. Hess, D. W. Keogh, L. A. Morales, M. P. Neu, W. Runde, C. D. Tait, D. K. Veirs, and P. M. Villella, Inorg. Chem. **42**, 3715 (2003).
[60]S. D. Conradson, B. D. Begg, D. L. Clark, C. den Auwer, M. Ding, P. K. Dorhout, F. J. Espinosa-Faller, P. L. Gordon, R. G. Haire, N. J. Hess, R. F. Hess, D. W. Keogh, L. A. Morales, M. P. Neu, P. Paviet-Hartmann, W. Runde, C. D. Tait, D. K. Veirs, and P. M. Villella, J. Am. Chem. Soc. **126**, 13443 (2004).
[61]D. Fausti, R. I. Tobey, N. Dean, S. Kaiser, A. Dienst, M. C. Hoffmann, S. Pyon, T. Takayama, H. Takagi, and A. Cavalleri, Science **331**, 189 (2011).
[62]Y. Q. An, A. J. Taylor, S. D. Conradson, S. A. Trugman, T. Durakiewicz, and G. Rodriguez, Phys. Rev. Lett. **106**, 207402 (2011).
[63]S. D. Conradson, I. D. Raistrick, and A. R. Bishop, Science **248**, 1394 (1990).
[64]T. Egami, B. H. Toby, S. J. L. Billinge, H. D. Rosenfeld, J. D. Jorgensen, D. G. Hinks, B. Dabrowski, M. A. Subramanian, M. K. Crawford, W. E. Farneth, and E. M. McCarron, Physica C **185**, 867 (1991).
[65]J. M. Deleon, S. D. Conradson, I. Batistic, A. R. Bishop, I. D. Raistrick, M. C. Aronson, and F. H. Garzon, Phys. Rev. B **45**, 2447 (1992).
[66]M. Arai, K. Yamada, S. Hosoya, A. C. Hannon, Y. Hidaka, A. D. Taylor, and Y. Endoh, J. Supercon. **7**, 415 (1994).
[67]M. I. Salkola, A. R. Bishop, S. A. Trugman, and J. M. Deleon, Phys. Rev. B **51**, 8878 (1995).
[68]A. Bianconi, N. L. Saini, T. Rossetti, A. Lanzara, A. Perali, M. Missori, H. Oyanagi, H. Yamaguchi, Y. Nishihara, and D. H. Ha, Phys. Rev. B **54**, 12018 (1996).
[69]A. Bussmann-Holder and A. R. Bishop, Phys. Rev. B **56**, 5297 (1997).

[70] S. D. Conradson, D. A. Andersson, P. S. Bagus, E. R. Batista, K. S. Boland, J. A. Bradley, D. D. Byler, D. L. Clark, D. R. Conradson, N. J. Hess, M. B. Martucci, R. L. Martin, D. Nordlund, G. T. Seidler, and X.-D. Wen, J. Am. Chem. Soc. (to be published).

[71] I. D. Prodan, G. E. Scuseria, and R. L. Martin, Phys. Rev. B **76**, 033101 (2007).

[72] J. M. Deleon, I. Batistic, A. R. Bishop, S. D. Conradson, and S. A. Trugman, Phys. Rev. Lett. **68**, 3236 (1992).

[73] M. I. Salkola, A. R. Bishop, J. M. Deleon, and S. A. Trugman, Phys. Rev. B **49**, 3671 (1994).

[74] J. M. DeLeon, S. D. Conradson, T. Tyson, A. R. Bishop, M. Salkola, F. J. Espinosa, and J. L. Pena, in *Applications of Synchrotron Radiation Techniques to Materials Science III*, edited by L. J. Terminello, S. M. Mini, H. Ade, and D. L. Perry (Materials Research Society, Warrendale, PA, 1996), Vol. 437, p. 189.

[75] M. P. A. Fisher, P. B. Weichman, G. Grinstein, and D. S. Fisher, Phys. Rev. B **40**, 546 (1989).

[76] M. Greiner, O. Mandel, T. Esslinger, T. W. Hansch, and I. Bloch, Nature **415**, 39 (2002).

[77] V. J. Wheeler, R. M. Dell, and E. Wait, J. Inorg. Nucl. Chem. **26**, 1829 (1964).

[78] R. G. Denning, J. C. Green, T. E. Hutchings, C. Dallera, A. Tagliaferri, K. Giarda, N. B. Brookes, and L. Braicovich, J. Chem Phys. **117**, 8008 (2002).

[79] See Supplemental Material at http://link.aps.org/supplemental/10.1103/PhysRevB.88.115135 for complete information on the results from the crystallographic and pdf refinements of the neutron and x-ray scattering data, the x-ray absorption data, and the original time-resolved optical pump-optical probe data.

[80] J. A. Bradley, P. Yang, E. R. Batista, K. S. Boland, C. J. Burns, D. L. Clark, S. D. Conradson, S. A. Kozimor, R. L. Martin, G. T. Seidler, B. L. Scott, D. K. Shuh, T. Tyliszczak, M. P. Wilkerson, and L. E. Wolfsberg, J. Am. Chem. Soc. **132**, 13914 (2010).

[81] J. A. Bradley, S. Sen Gupta, G. T. Seidler, K. T. Moore, M. W. Haverkort, G. A. Sawatzky, S. D. Conradson, D. L. Clark, S. A. Kozimor, and K. S. Boland, Phys. Rev. B **81**, 193104 (2010).

[82] I.-K. Jeong, J. Thompson, T. E. Proffen, A. M. P. Turner, and S. J. L. Billinge, J. Appl. Crystallogr. **34**, 536 (2001).

[83] P. F. Peterson, M. Gutmann, T. Proffen, and S. J. L. Billinge, J. Appl. Crystallogr. **33**, 1192 (2000).

[84] C. L. Farrow, P. Juhas, J. W. Liu, D. Bryndin, E. S. Bozin, J. Bloch, T. Proffen, and S. J. L. Billinge, J. Phys.: Condens. Matter **19**, 335219 (2007).

[85] A. C. Larson and R. B. Von Dreele, Los Alamos National Laboratory Report 86-748, 2004.

[86] S. I. Zabinsky, J. J. Rehr, A. Ankudinov, R. C. Albers, and M. J. Eller, Phys. Rev. B **52**, 2995 (1995).

[87] A. L. Ankudinov, B. Ravel, J. J. Rehr, and S. D. Conradson, Phys. Rev. B **58**, 7565 (1998).

[88] T. T. Fister, G. T. Seidler, L. Wharton, A. R. Battle, T. B. Ellis, J. O. Cross, A. T. Macrander, W. T. Elam, T. A. Tyson, and Q. Qian, Rev. Sci. Instrum. **77**, 063901 (2006).

[89] T. T. Fister, G. T. Seidler, C. Hamner, J. O. Cross, J. A. Soininen, and J. J. Rehr, Phys. Rev. B **74**, 214117 (2006).

[90] G. Kresse and J. Hafner, Phys. Rev. B **48**, 13115 (1993).

[91] G. Kresse and J. Furthmuller, Phys. Rev. B **54**, 11169 (1996).

[92] G. Kresse and J. Furthmuller, Comp. Mater. Sci. **6**, 15 (1996).

[93] G. Kresse and D. Joubert, Phys. Rev. B **59**, 1758 (1999).

[94] P. E. Blochl, Phys. Rev. B **50**, 17953 (1994).

[95] A. I. Liechtenstein, V. I. Anisimov, and J. Zaanen, Phys. Rev. B **52**, R5467 (1995).

[96] S. L. Dudarev, D. N. Manh, and A. P. Sutton, Philos. Mag. B **75**, 613 (1997).

[97] B. Dorado, B. Amadon, M. Freyss, and M. Bertolus, Phys. Rev. B **79**, 235125 (2009).

[98] B. Meredig, A. Thompson, H. A. Hansen, C. Wolverton, and A. van de Walle, Phys. Rev. B **82**, 195128 (2010).

[99] F. Jollet, T. Petit, S. Gota, N. Thromat, M. GautierSoyer, and A. Pasturel, J. Phys.: Condens. Matter **9**, 9393 (1997).

[100] M. T. Paffett, D. Kelly, S. A. Joyce, J. Morris, and K. Veirs, J. Nucl. Mater. **322**, 45 (2003).

[101] J. Stultz, M. T. Paffett, and S. A. Joyce, J. Phys. Chem. B **108**, 2362 (2004).

[102] M. Magnuson, S. M. Butorin, L. Werme, J. Nordgren, K. E. Ivanov, J. H. Guo, and D. K. Shuh, Appl. Surf. Sci. **252**, 5615 (2006).

[103] A. Modin, Y. Yun, M. T. Suzuki, J. Vegelius, L. Werme, J. Nordgren, P. M. Oppeneer, and S. M. Butorin, Phys. Rev. B **83**, 075113 (2011).

[104] Z. Y. Wu, F. Jollet, S. Gota, N. Thromat, M. Gautier-Soyer, and T. Petit, J. Phys.: Condens. Matter **11**, 7185 (1999).

[105] R. K. Maccrone, S. Sankaran, S. R. Shatynski, and C. A. Colmenares, Metall. Trans. A **17**, 911 (1986).

[106] D. J. M. Bevan, O. Greis, and J. Strahle, Acta Crystallogr. A **36**, 889 (1980).

[107] D. Manara and B. Renker, J. Nucl. Mater. **321**, 233 (2003).

[108] T. Livneh and E. Sterer, Phys. Rev. B **73**, 085118 (2006).

[109] M. L. Palacios and S. H. Taylor, Appl. Spectrosc. **54**, 1372 (2000).

[110] J. A. Danis, M. R. Lin, B. L. Scott, B. W. Eichhorn, and W. H. Runde, Inorg. Chem. **40**, 3389 (2001).

[111] T. Ishii, K. Naito, and K. Oshima, J. Nucl. Mater. **36**, 288 (1970).

[112] V. V. Kabanov, J. Demsar, and D. Mihailovic, Phys. Rev. B **61**, 1477 (2000).

[113] R. D. Averitt and A. J. Taylor, J. Phys.-Condens. Matter **14**, R1357 (2002).

[114] A. J. Taylor, R. D. Averitt, J. Demsar, A. I. Lobad, J. L. Sarrao, and S. A. Trugman, Physica B **312**, 640 (2002).

[115] M. J. Haire, T. T. Meek, and B. G. von Roedern, Trans. Am. Nucl. Soc. **87**, 504 (2002).

[116] A. Arrott and J. E. Goldman, Phys. Rev. **108**, 948 (1957).

[117] M. J. M. Leask, W. P. Wolf, A. J. Walter, and L. E. J. Roberts, J. Chem. Soc. **20**, 4788 (1963).

[118] J. M. Deleon, S. D. Conradson, I. Batistic, and A. R. Bishop, Phys. Rev. Lett. **65**, 1675 (1990).

[119] C. Kuebler, H. Ehrke, R. Huber, R. Lopez, A. Halabica, R. F. Haglund, Jr., and A. Leitenstorfer, Phys. Rev. Lett. **99**, 116401 (2007).

[120] J. Demsar, K. Biljakovic, and D. Mihailovic, Phys. Rev. Lett. **83**, 800 (1999).

[121] R. V. Yusupov, T. Mertelj, J. H. Chu, I. R. Fisher, and D. Mihailovic, Phys. Rev. Lett. **101**, 246402 (2008).

[122] R. Yusupov, T. Mertelj, V. V. Kabanov, S. Brazovskii, P. Kusar, J. H. Chu, I. R. Fisher, and D. Mihailovic, Nat. Phys. **6**, 681 (2010).

[123] W. J. Siekhaus and A. Nelson, in *Actinides 2005–Basic Science, Applications and Technology*, edited by J. L. Sarrao, A. J. Schwartz, M. R. Antonio, P. C. Burns, R. G. Haire, and H. Nitsche, Mater. Res. Soc. Symp. Proc. 893 (Materials Research Society, Warrendale, PA, 2006), p. 349.

[124]Q. Y. Chen, X. C. Lai, T. Tang, B. Bai, M. F. Chu, Y. B. Zhang, and S. Y. Tan, J. Nucl. Mater. **401**, 118 (2010).
[125]T. R. Griffiths and H. V. S. Hubbard, J. Nucl. Mater. **185**, 243 (1991).
[126]T. T. Meek, B. von Roedern, P. G. Clem, and R. J. Hanrahan, Mater. Lett. **59**, 1085 (2005).
[127]M. Hangyo, M. Tani, and T. Nagashima, Int. J. Infrared Milli. **26**, 1661 (2005).
[128]G. Dolling, R. A. Cowley, and A. D. B. Woods, Can. J. Phys. **43**, 1397 (1965).
[129]J. E. Peralta, J. Heyd, G. E. Scuseria, and R. L. Martin, Phys. Rev. B **74**, 073101 (2006).
[130]L. Rao, J. G. Tobin, and D. K. Shuh, IOP. Conf. Ser.: Mater. Sci. Eng. **9**, 011001 (2010).
[131]R. D. Averitt, A. I. Lobad, C. Kwon, S. A. Trugman, V. K. Thorsmolle, and A. J. Taylor, Phys. Rev. Lett. **87**, 017401 (2001).
[132]L. H. Palmer and M. Tinkham, Phys. Rev. **165**, 588 (1968).
[133]M. C. Nuss, K. W. Goossen, J. P. Gordon, P. M. Mankiewich, M. L. Omalley, and M. Bhushan, J. Appl. Phys. **70**, 2238 (1991).
[134]M. C. Nuss, P. M. Mankiewich, M. L. Omalley, E. H. Westerwick, and P. B. Littlewood, Phys. Rev. Lett. **66**, 3305 (1991).
[135]R. D. Averitt, G. Rodriguez, A. I. Lobad, J. L. W. Siders, S. A. Trugman, and A. J. Taylor, Phys. Rev. B **63**, 140502 (2001).
[136]D. J. Hilton, R. P. Prasankumar, S. A. Trugman, A. J. Taylor, and R. D. Averitt, J. Phys. Soc. Jpn. **75**, 011006 (2006).
[137]J. M. Tranquada, B. J. Sternlieb, J. D. Axe, Y. Nakamura, and S. Uchida, Nature **375**, 561 (1995).
[138]A. Moreo, S. Yunoki, and E. Dagotto, Science **283**, 2034 (1999).
[139]F. V. Kusmartsev, D. Di Castro, G. Bianconi, and A. Bianconi, Phys. Lett. A **275**, 118 (2000).
[140]Z. A. Xu, N. P. Ong, Y. Wang, T. Kakeshita, and S. Uchida, Nature **406**, 486 (2000).
[141]J. M. Tranquada, K. Nakajima, M. Braden, L. Pintschovius, and R. J. McQueeney, Phys. Rev. Lett. **88**, 075505 (2002).
[142]M. Fratini, N. Poccia, A. Ricci, G. Campi, M. Burghammer, G. Aeppli, and A. Bianconi, Nature **466**, 841 (2010).
[143]J. A. Slezak, J. Lee and J. C. Davis, MRS Bull. **30**, 437 (2005).
[144]A. Mesaros, K. Fujita, H. Eisaki, S. Uchida, J. C. Davis, S. Sachdev, J. Zaanen, M. J. Lawler, and E.-A. Kim, Science **333**, 426 (2011).
[145]I. B. Bersuker, *The Jahn-Teller Effect* (Cambridge University Press, New York, 2006).
[146]G. M. Watson, B. D. Gaulin, D. Gibbs, T. R. Thurston, P. J. Simpson, S. M. Shapiro, G. H. Lander, H. Matzke, S. Wang, and M. Dudley, Phys. Rev. B **53**, 686 (1996).
[147]R. Osborn, Physica B **159**, 151 (1989).
[148]P. Piekarz and T. Egami, Phys. Rev. B **72**, 054530 (2005).
[149]Y. Yun, D. Legut, and P. M. Oppeneer, J. Nucl. Mater. **426**, 109 (2012).
[150]M. Albiez, R. Gati, J. Folling, S. Hunsmann, M. Cristiani, and M. K. Oberthaler, Phys. Rev. Lett. **95**, 010402 (2005).
[151]K. A. Al-Hassanieh, F. A. Reboredo, A. E. Feiguin, I. Gonzalez, and E. Dagotto, Phys. Rev. Lett. **100**, 166403 (2008).